Consortium for Small-Scale Modelling

Newsletter

July 2017 *No. 17*

Deutscher Wetterdienst

Ufficio Generale Spazio Aereo e Meteorologia

Instytucie Meteorogii i Gospodarki Wodnej

Agenzia Regionale per la Protezione Ambientale dell'Emilia Romagna Servizio Idro Meteo Clima

Centro Italiano Ricerche Aerospaziali

Israel Meteorological Service

MeteoSwiss

ΕΘΝΙΚΗ ΜΕΤΕΩΡΟΛΟΓΙΚΗ ΥΠΗΡΕΣΙΑ

Administratia Nationala de Meteorologie

Federal Service for Hydrometeorology and Environmental Monitoring

Amt fur GeoInformationswesen der Bundeswehr

Agenzia Regionale per la Protezione Ambientale del Piemonte

www.cosmo-model.org

Editors: Mihaela Bogdan (NMA); Massimo Milelli (ARPA-Piedmont); Ulrich Schattler (DWD);

Table of Contents

The current issue of the COSMO Newsletter contains five contributions that cover some aspects of the R&D efforts undertaken in the Consortium for Small-Scale Modelling. All contributors to the COSMO Newsletter No. 17 are gratefully acknowledged. Extensive discussions of the various COSMO issues (including recent achievements, pressing problems, future challenges, and management) took place during the 18th COSMO General Meeting held 5-8 September 2016 in Offenbach, Germany.Details can be found at the COSMO web page *http://www.cosmo-model.org/content/consortium/generalMeetings/general2016/default.htm*

One recent event should be particularly mentioned. In 2017, COSMO wholeheartedly welcomed a new member, namely, the Israel Meteorological Service (IMS). The IMS colleagues are already making important contributions to a number of COSMO projects, and I am sure will further strengthen their role in COSMO in the future.

Guided by the COSMO Strategy and the COSMO Science Plan, the Consortium strives to improve the weather forecast and to maintain high satisfaction of its numerous customers. Much effort nowadays goes into the convection-permitting scales and the ensemble prediction systems. Mention should be made of the recently completed COSMO Priority Project KENDA that resulted in the development and implementation of the novel ensemble data assimilation system based on the Local Ensemble Transform Kalman Filter (LETKF). The LETKF-based data assimilation system (KENDA) became operational at DWD in March 2017 (for both ensemble and deterministic forecasts) and at ARPAE in May 2017 (for deterministic forecast only). Recall that MCH has been running KENDA operationally since May 2016 (for ensemble forecast). Other Consortium members are expected to consider the operational use of KENDA in the not too distant future. Within the framework of the COSMO working groups, priority projects and priority tasks, the COSMO scientists deal with a number of pressing problems that are high on the agenda of the NWP centres. These include development of dynamical cores with improved conservation properties; more intimate coupling of turbulence, microphysics, radiation and soil (including ocean and lakes) parameterization schemes; development and efficient use of spatial verification methods for ensemble and deterministic forecasts; representation of model uncertainties and development of perturbation methods for the ensemble prediction systems; development of objective and efficient methods of calibration of NWP models; and performance on the massively parallel (e.g. GPU-based) computer architectures. COSMO also pays much attention to the COSMO software maintenance and to comprehensive testing and timely release of new model versions. The release notes are found at the COSMO web page, *http://www.cosmo-model.org*. Last but not the least, the unification of (parts of) the codes of the NWP models COSMO and ICON looms large on the COSMO agenda, and much effort is made along this line. Considerable progress has been made in the development of common COSMO-ICON library of physical parameterization schemes. More information about the COSMO activities can be found at the COSMO web page.

COSMO currently faces a number of strong challenges. One well-known and very challenging issue is related to the resolution at which convection is (arguably) permitted but not yet resolved. Apart from this issue that calls for significant research effort, the Consortium urgently needs to solve some problems of both R&D and management character. These include the future of the COSMO Working Group 4 "Interpretation and Applications" that is fairly uncertain at the time being, and further development and restructuring of the Meteorological Test Suite that is crucial for timely release of new COSMO-model versions. The above and many other issues will be discussed at the next COSMO General Meeting to be held in Jerusalem, Israel, 11-14 September 2017.

Enjoy your work in COSMO and the COSMO spirit!

Dmitrii Mironov
COSMO Scientific Project Manager

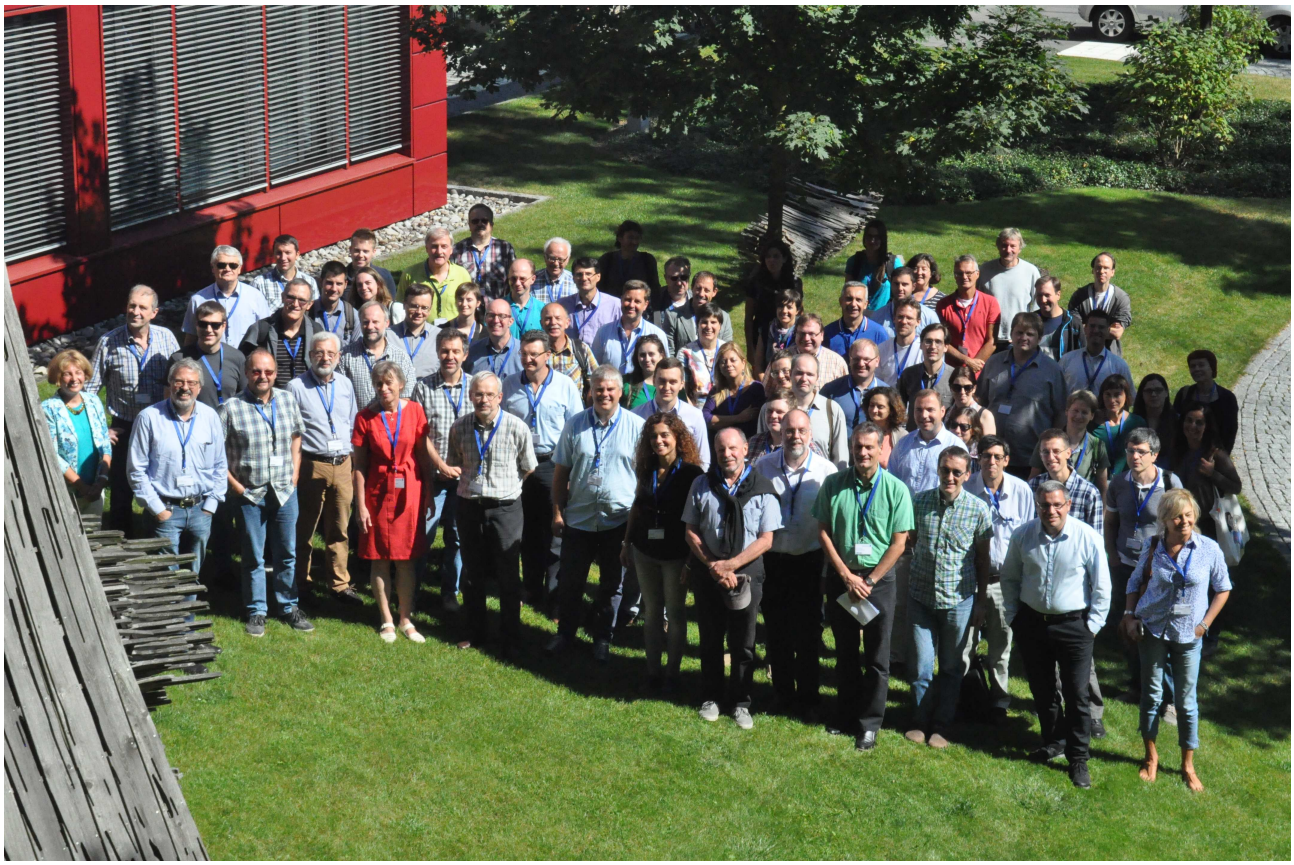

Figure 1: Participants of the 16th COSMO General Meeting in Offenbach

Preliminary activity with COSMO-1 over Torino including TERRA-URB parameterisation

M. Milelli[1], E. Bucchignani[2,3], P. Mercogliano[2,3], V. Garbero[1]

1 ARPA Piemonte (Torino, Italy), 2 CIRA (Capua, Italy), 3 CMCC (Capua, Italy)

1 Introduction

The modeling of urban environment has gained much attention in the last years; in fact, multiple parameterisations for the land use type have been developed. The bulk schemes take into account the overall radiative, thermal, turbulent-transfer properties, and water-storage capacity of the urban canopy with a set of bulk parameters. These model parameters are estimated from model sensitivity experiments. The bulk schemes are suitable for capturing the general characteristics of the urban climate in regional climate modeling in an efficient way. However, they do not explicitly resolve the complex processes depending on the local characteristics of the urban canopy, which further modulate the urban climate. The explicit canyon schemes explicitly capture the complex physical processes depending on the local characteristics of the urban canopy, which further modulate the urban climate. Yet, the applicability of these explicit-canyon schemes for atmospheric modeling is sometimes limited by either the lack of detailed urban canopy information, computational cost and their model complexity.

In COSMO model, cities are represented by natural land surfaces with an increased surface roughness length and a reduced vegetation cover (modification of soil and vegetation parameters of the TERRA model). However, in this representation, urban areas are still treated as water-permeable soil with aerodynamic, radiative and thermal parameters similar to the surrounding natural land. Therefore, this basic representation could not reliably capture the urban physics and associated urban-climatic effects including urban heat islands. For this reason, further developments of the parameterisation of the urban land have been carried out. In particular, the TERRA-URB bulk parameterisation scheme with a prescribed anthropogenic heat flux has been used in this work (see [1] and [2] for details). The simple bulk-model TERRA-URB includes the effects of buildings on the air flow without resolving the energy budgets of the buildings themselves, but using the externally calculated anthropogenic heat flux. This approach allows representing effects of multiple cities on the atmosphere without requiring additional data on the building structure. The use of the previously estimated anthropogenic heat flux, modified thermal and radiative parameters and a modified surface-layer transfer scheme, provides the urban heat island with the correct diurnal phase. The magnitude of this flux can potentially be revised to fit the mean measured signal. TERRA-URB uses a pre-calculated anthropogenic heat flux (Q_F), which accounts for country-specific data of energy consumption, calculated on the base of the population density and the latitude dependent diurnal and seasonal distribution. Due to this simple representation of the urban land as a bulk, TERRA-URB is computationally inexpensive. The latest version of TERRA-URB implements the Semi-empirical Urban canopy parameterization (SURY). It translates urban-canopy parameters (containing 3D information) into bulk parameters. TERRA-URB takes additional surface parameter input fields: ISA (Impervious Surface Area) and AHF (Annual-mean anthropogenic Heat Flux), generated with EXTPAR via the WebPEP interface. By default, TERRA-URB takes fixed values for the urban canopy parameters: variation of urban-canopy parameters is optional.

2 Test case and model setup

In the period 1-16 July 2015, Piemonte region and Torino in particular experienced extreme temperature values and uncomfortable conditions for the population. In particular July 2015 has been the hottest July since 1958 (Fig. 1). For more information regarding the climatological analysis and the methodology, see [4] (in Italian). It comes out that July 2015 is ranked first in all the measurements. In Torino, the maximum temperature reached 38.5°C during that period and ground stations data pointed out the presence of a clear UHI effect. This is the reason why this area and this period represent a suitable benchmark to test the capabilities of COSMO, and in particular of the urban parameterization. The analysis follows the study published in the COSMO Newsletter 16 ([3]) so the same stations have been considered: Torino Consolata (urban), Torino Giardini Reali (urban park) and Moncalieri Bauducchi (rural) (see Fig. 2 and Tab. 1).

The model setup is the following:

- COSMO resolution: 0.009° (about 1 km);

name	lat	lon
Moncalieri/Bauducchi (rural)	44.961111°	7.709227°
Giardini Reali (urban park)	45.073699°	7.688576°
Consolata (urban)	45.076667°	7.679444°

Table 1: List of stations used.

	AHF (W/m^2)	ISA	URBAN	H (m)	Soil Type
Bauducchi	3	0.061	0	225	6
Consolata	23.6	0.91	1	232	6
Giardini Reali	15.3	0.825	1	230	6

Table 2: Values of some variable in the selected points.

- computational domain: 100 x 100 points, 60 vertical levels, time step 3 s (see Fig. 3);
- time period: from 1 to 7 July 2015;
- forcing data: IFS analysis (resolution of 0.075°).

The simulations have been performed according to the following prospect:

- NON-URB: simulation with TERRA-URB off;
- URB: simulation with TERRA-URB on.

The maps of few important parameters are shown in Fig. 4 and the single values correspondent to the single point are listed in the Tab. 2. The model considers Moncalieri Bauducchi a rural station and the other two urban stations (correctly).

3 Results

The time series of observed T2m in the three stations are plotted in Fig. 5 with the model output (URB and NON-URB). A general overview confirms that in Consolata the daily maxima are slightly overestimated by URB, while the minima are better than the operational (NON-URB). In Giardini Reali the maxima are nicely simulated by URB while the minima are overestimated (NON-URB is better). As expected there are no significant differences between URB and NON-URB simulations in rural areas, that is both underestimate the maxima and overestimate the minima.

Tab. 3 shows the average observed T2m value and the average bias (model minus observation) related to the basic simulations. URB allows a reduction of the average bias compared with NON-URB in Consolata and in Moncalieri, while in Giardini Reali the trend is opposite.

In Fig. 6 the soil surface temperature time series are shown. While there is basically no change in rural areas (Moncalieri), there is a large modification in the city with a general increase, especially in the maxima values.

	Obs	Bias Urb	Bias Non-urb
Consolata	29.4	0.68	-1.22
Moncalieri	28.2	-0.55	-0.74
Giardini Reali	28.7	1.37	-0.59

Table 3: Mean observed T2m values and mean model bias.

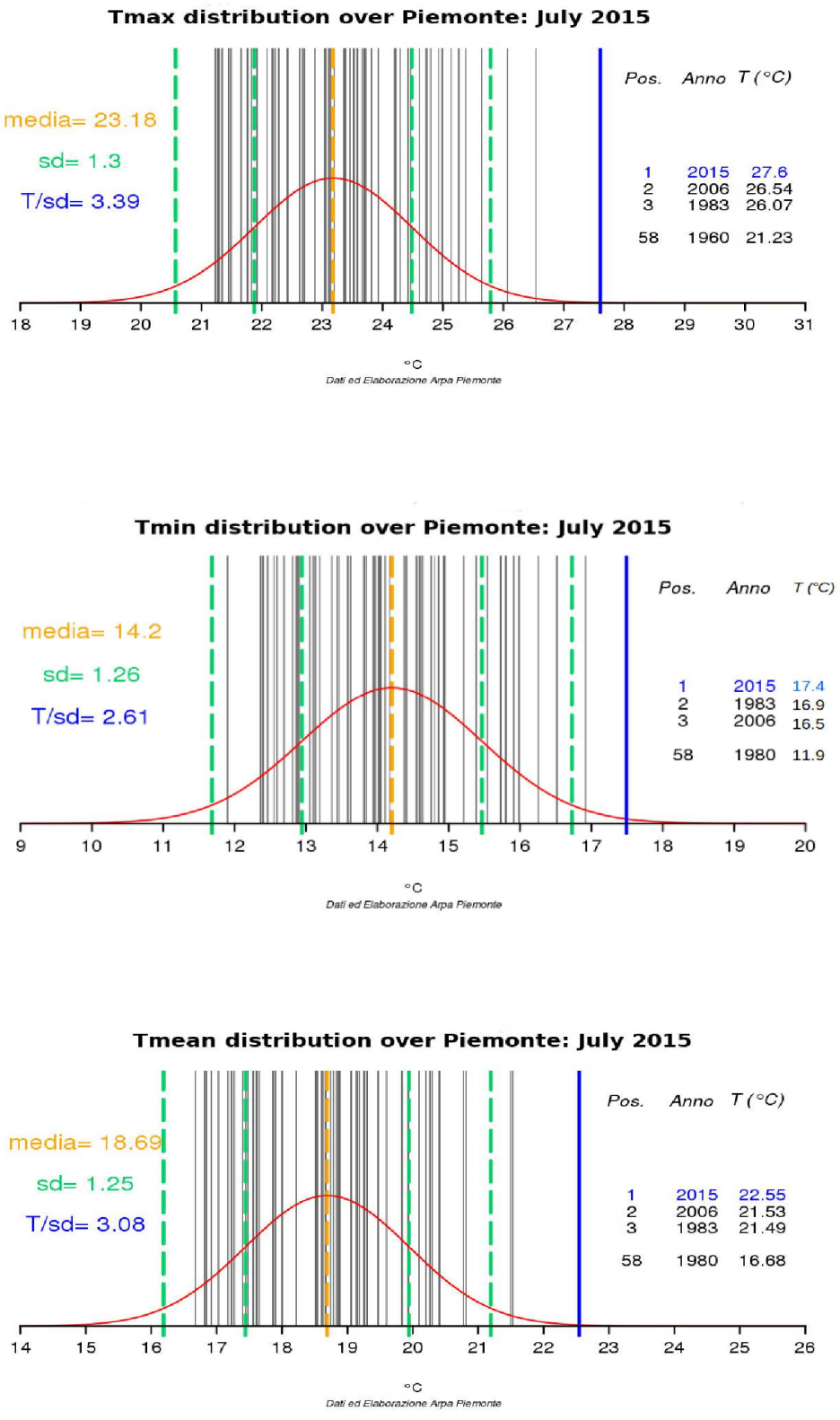

Figure 1: Distribution of T2m max (top), min (middle) and mean (bottom) in July 2015 over Piemonte.

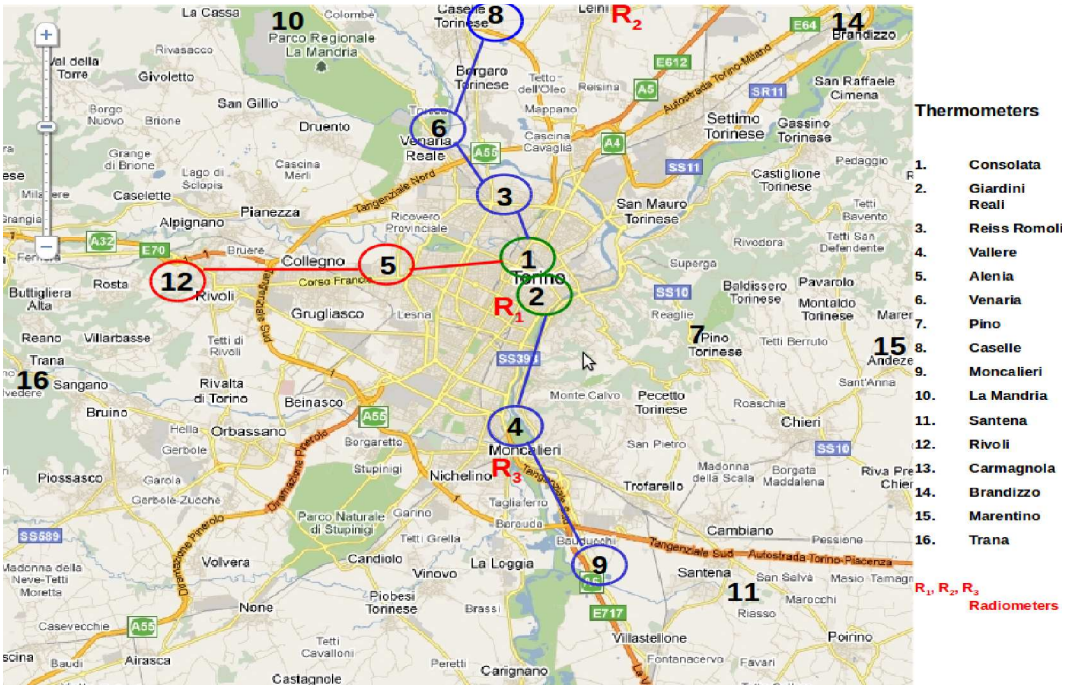

Figure 2: Location of the three observation stations considered in the Torino area (1, 2 and 9).

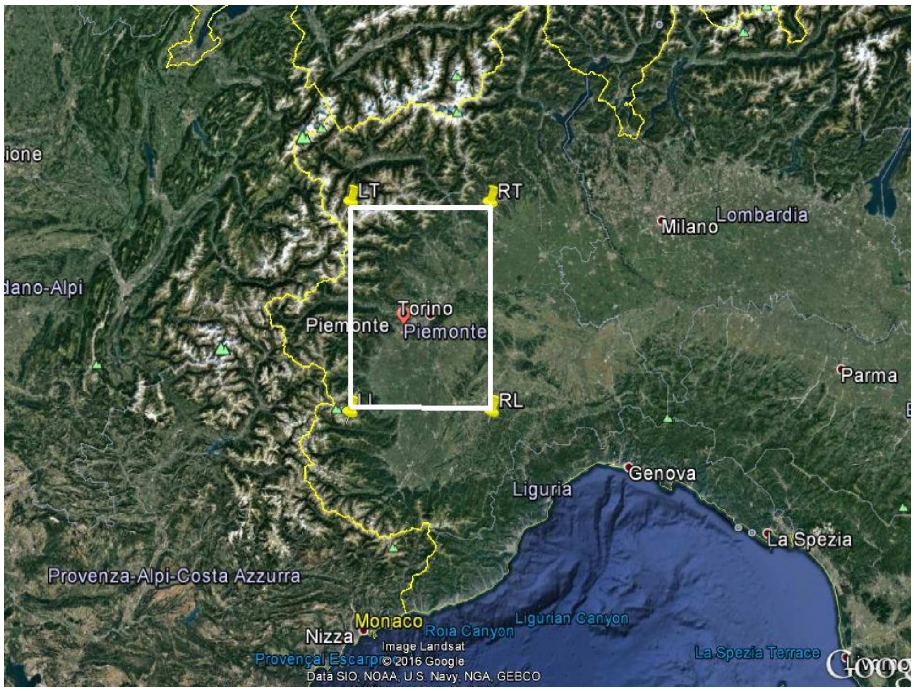

Figure 3: The computational domain.

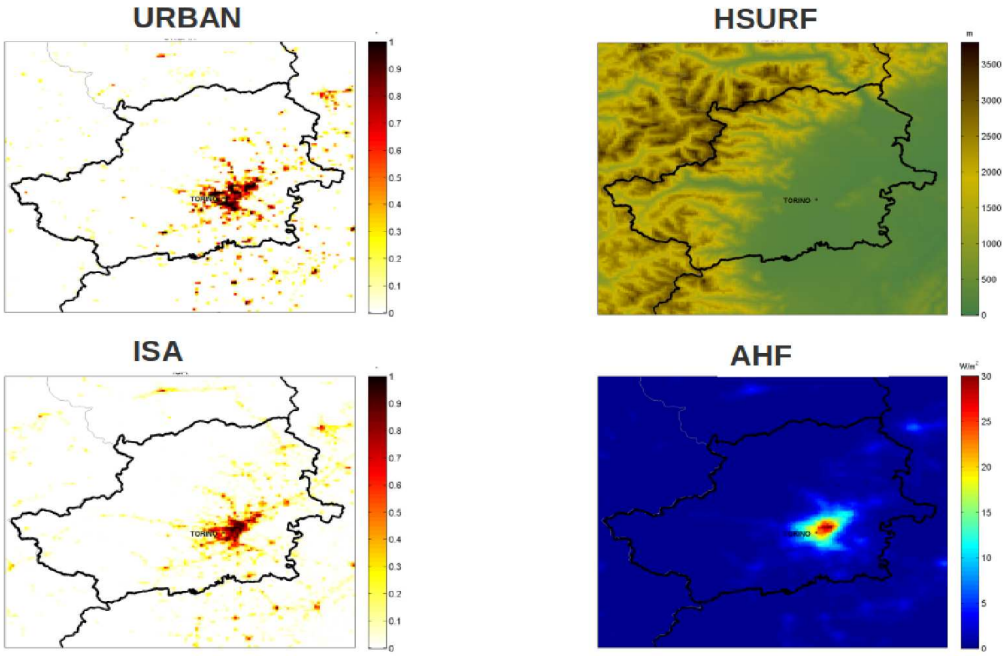

Figure 4: Distribution of the additional parameters over the area.

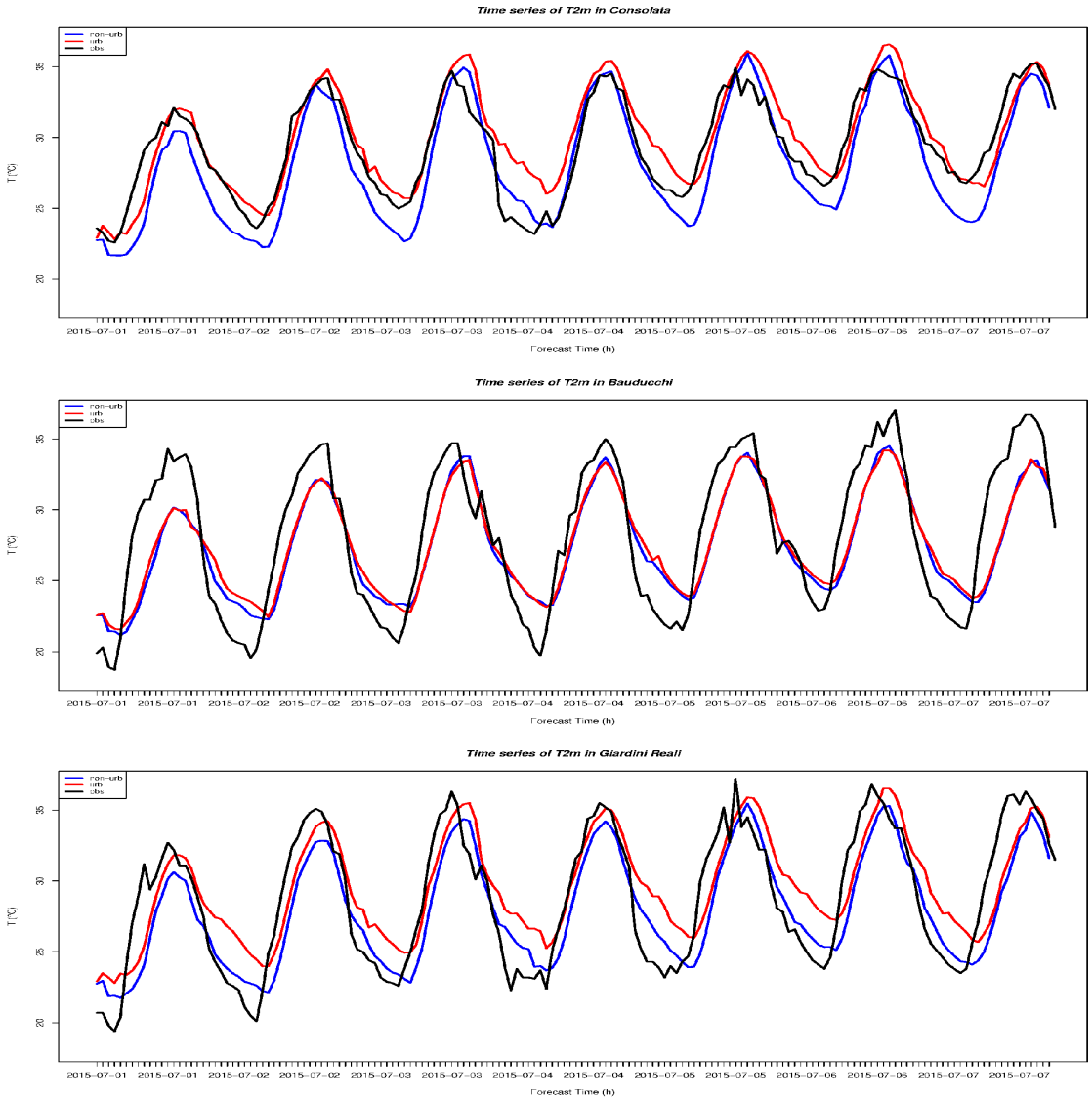

Figure 5: Time series T2m for Consolata station (urban cell, top), Moncalieri Bauducchi (rural, middle) and Torino Giardini Reali (urban, bottom) with the different simulations and observed data.

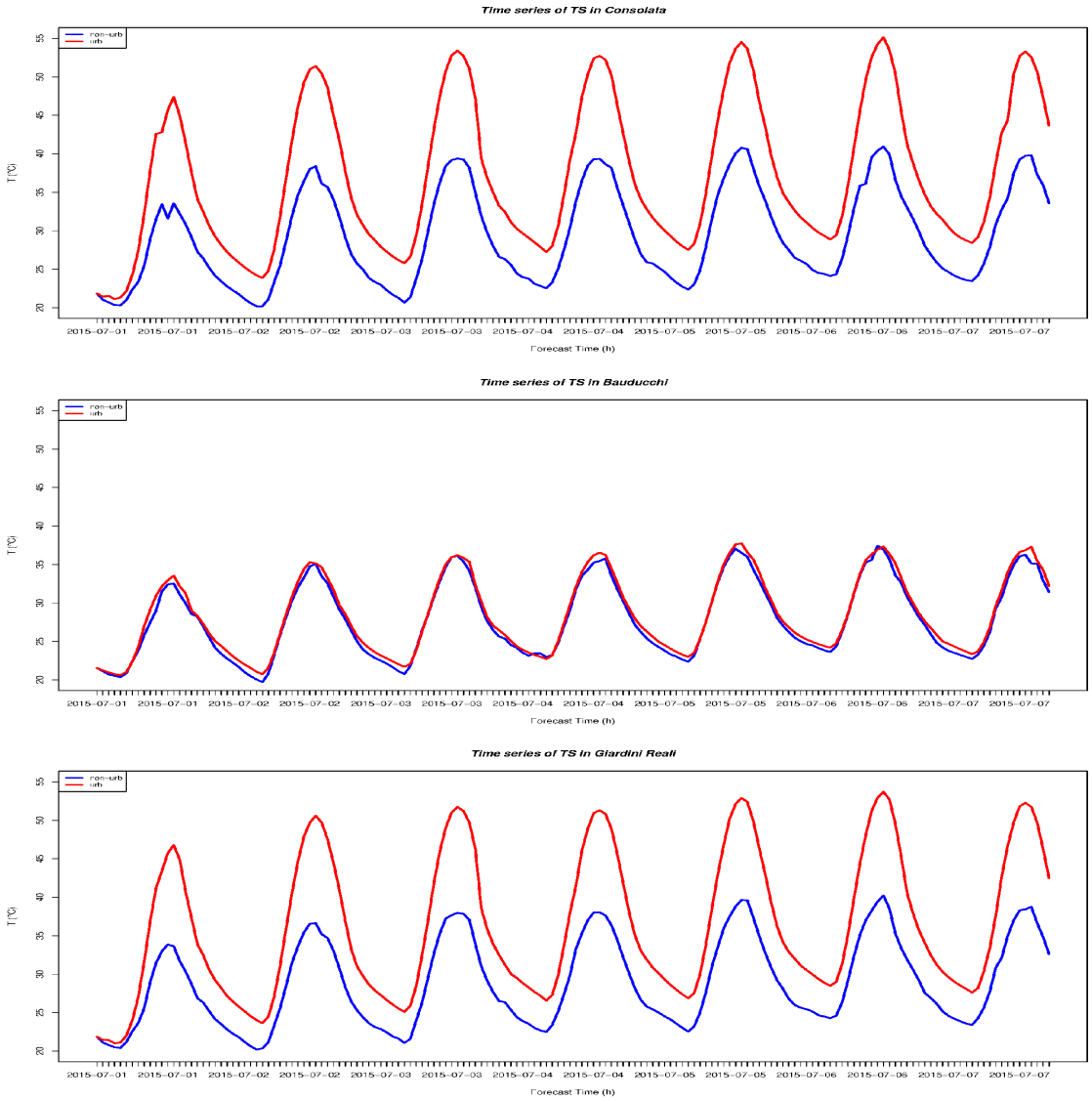

Figure 6: Time series of T_S (soil surface T) for Consolata station (top), and Moncalieri (middle) and Giardini Reali (bottom) with the different simulations.

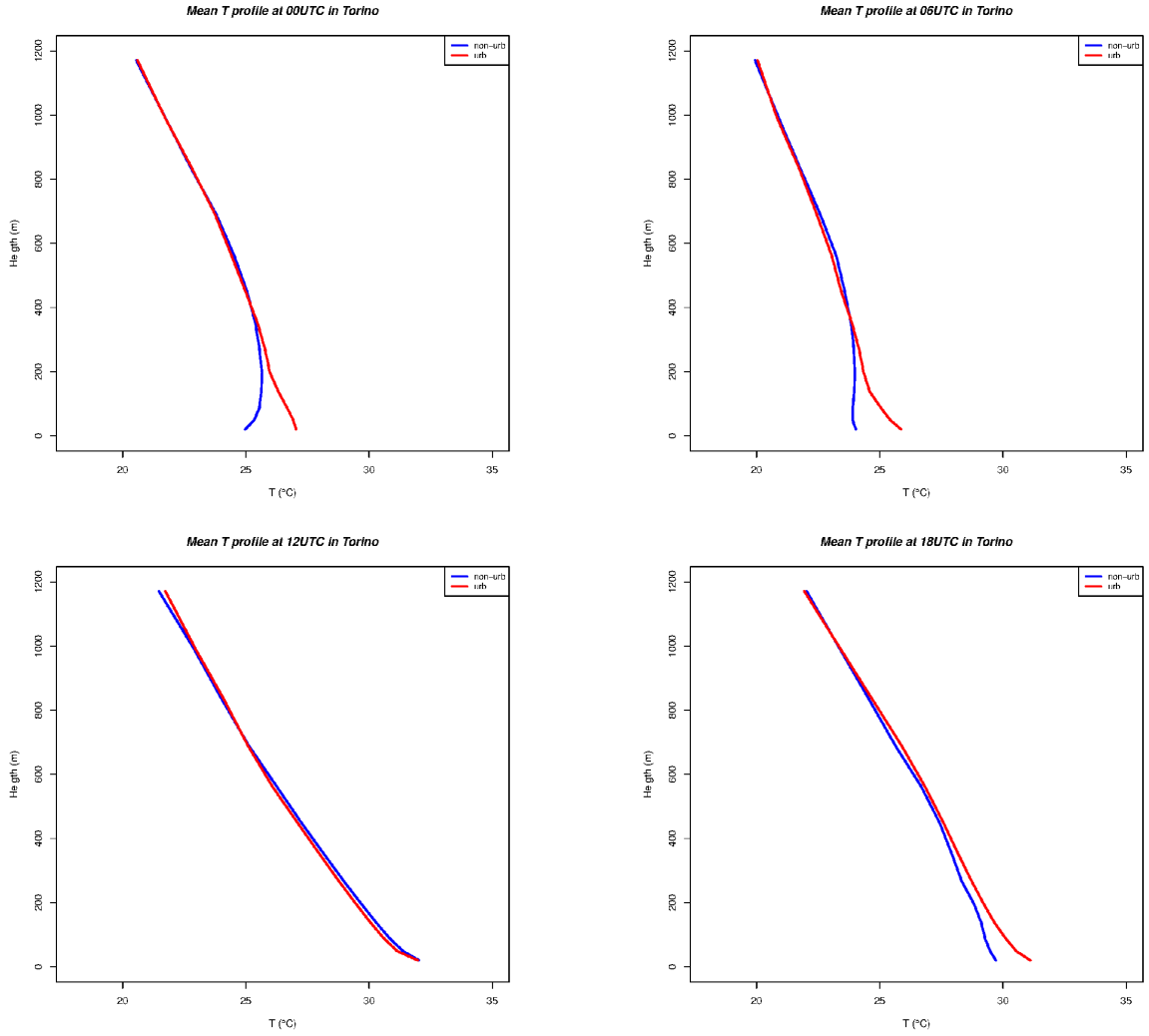

Figure 7: Mean vertical profile of T over Torino Consolata at different hours.

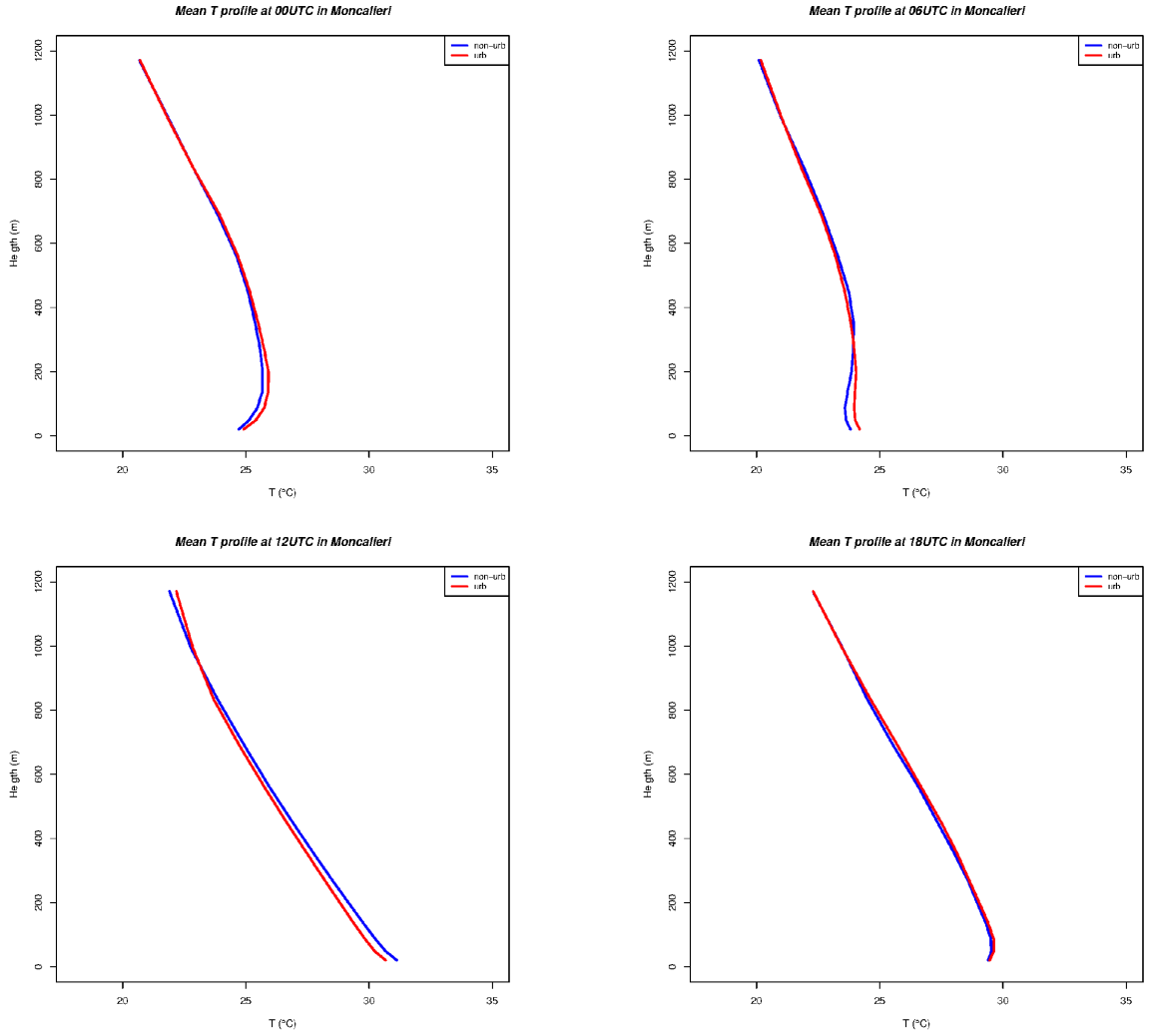

Figure 8: Mean vertical profile of T over Moncalieri Bauducchi at different hours.

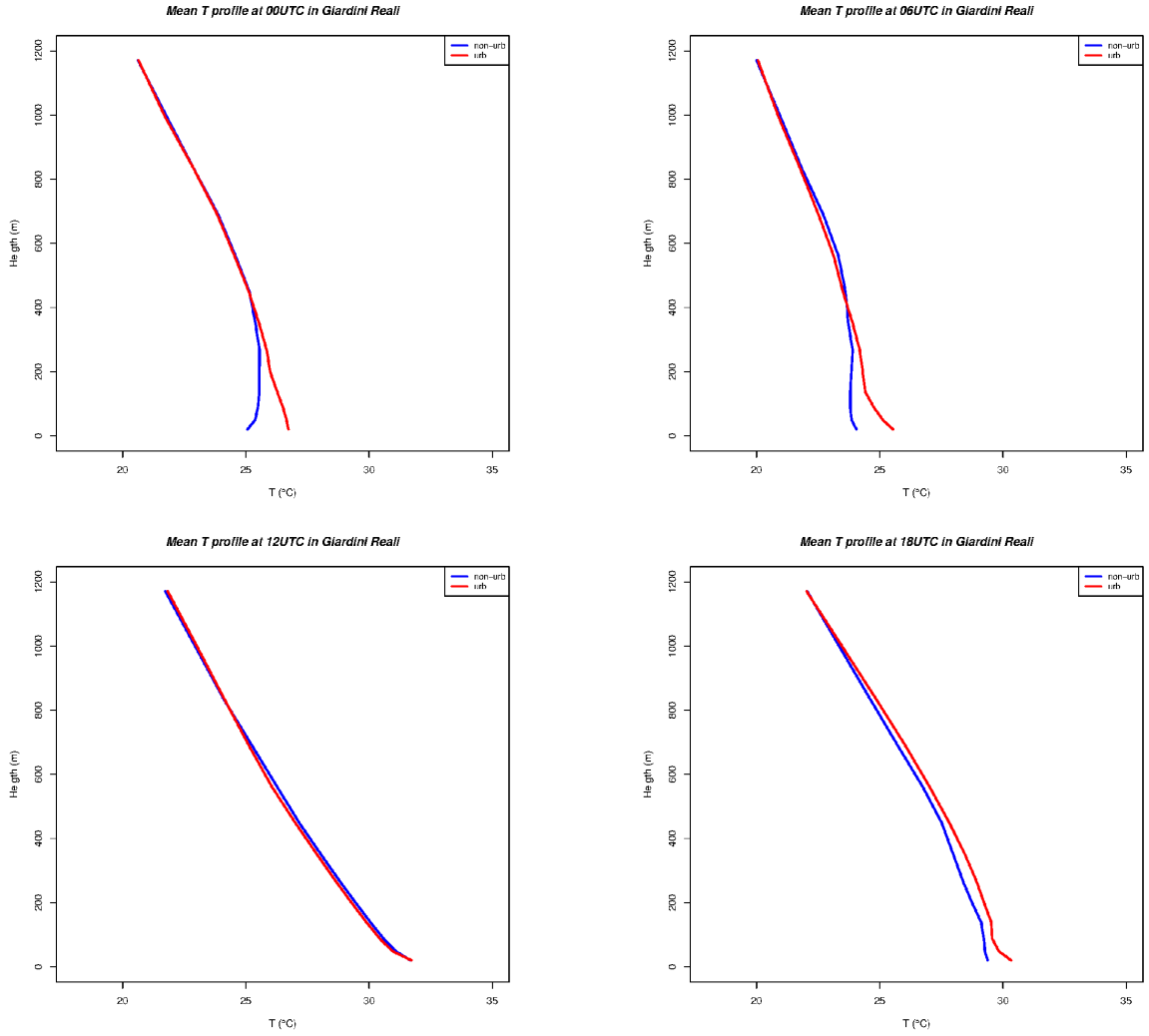

Figure 9: Mean vertical profile of T over Torino Giardini Reali at different hours.

The simulated vertical profiles of T are shown in Figs. 7-9. In Torino Consolata the difference between URB and NON-URB is limited to the lowest layers where URB has in general higher temperatures (except at 12UTC where the profiles are equivalent). Above 300-400 m the profiles collapse to a single curve. In Moncalieri (rural area) the differences are quite small as it could be expected. Torino Giardini Reali is quite similar to Consolata.

4 Summary and outlook

A set of simulations have been performed with COSMO over Torino area at very high resolutions (about 1 km), considering the period 1-7 July 2015. The bulk model TERRA-URB parameterizes the effects of buildings on the air flow using the externally calculated anthropogenic heat flux. The effects of the introduction of this urban parameterization on the quality of results have been quantified. TERRA-URB allows a better representation of the daily minimum temperature. This is a remarkable results, since it is the minimum temperature that determines the UHI (mainly). However, considerable work is still needed, especially for what concerns the optimization of the model configuration. This work has been performed with a private version of COSMO, modified with TERRA-URB, but once the scheme will be included in the official COSMO release (v5.6), a more structured project will start.

Hendrik Wouters (KU Leuven, Belgium) and Uli Blahak (DWD) are gratefully acknowledged for providing the COSMO/TERRA-URB software package and for the technical and scientific hints.

We would like to thank the Italian National Department of Civil Protection for the support given to this project.

References

[1] Wouters, H., Demuzere M., Ridder K. D. and van Lipzig N. P., 2015: The impact of impervious water-storage parametrization on urban climate modelling. *Urban Climate*, 11, **24–50**.

[2] Wouters, H., Demuzere, M., Blahak, U., Fortuniak, K., Maiheu, B., Camps, J., Tielemans, D. and van Lipzig, N. P. M., 2016: The efficient urban canopy dependency parametrization (SURY) v1.0 for atmospheric modelling: description and application with the COSMO-CLM model for a Belgian summer. *Geosci. Model Dev.*, 9, **3027-3054**.

[3] Milelli, M., 2016: Urban heat island effects over Torino. *COSMO Newsletter*, 16, **1-10**.

[4] http://www.arpa.piemonte.gov.it/rischinaturali/tematismi/clima/confronti-storici/dati/dati.html

Urban wind analysis in Warsaw

Katarzyna Starosta, Andrzej Wyszogrodzki

Department of COSMO Numerical Weather Prediction National Center for Meteorological Protection Institute of Meteorology and Water Management – National Research Institute. PL-01-673 Warsaw, 61 Podleśna str.
katarzyna.starosta@imgw.pl; andrzej.wyszogrodzki@imgw.pl

1 Introduction

The population of large urban areas is growing rapidly. By 2050 it is predicted that two-third of global population will be the city inhabitants. As the cities constantly grow the high-end technology is being utilized to manage urban development, which leads to the concept of Smart Cities - friendly and intelligent infrastructure for their citizens.

One of the key factors of Smart City concept is the promotion of green energy from renewable sources, another important problem for cities is the smog and air pollution. A high quality wind conditions form weather forecasting model may be necessary to calculate the ventilation index for the different city areas.

The aim of this work is to provide assessment of the use of numerical weather prediction (NWP) models for wind speed and wind direction forecasting in the urban space. Roughness length is an important concept in urban meteorology, accounting for the structure and type of buildings, roads, parks and rivers within the city area. These parameters are affecting meteorological conditions as winds which are the single most important source of free kinetic energy and a major factor determining the urban air quality.

For further practical use, the forecast data from numerical model COSMO at 2.8 resolution has to be verified with the data from urban meteorological stations. In this work we use the 2015 year data from two WMO network stations located in Warsaw at Okęcie and Bielany. The Okęcie station is located at the Okęcie airport in the south-western suburbs of the city, while the station Bielany is located in the northern part of the city in the valley of the Vistula River.

These locations were chosen to account for an impact of the city structure on the daily course of wind speed and wind direction. Detailed calculations and analyzes of observational and COSMO wind data were performed for the whole 2015 year, accounting for the annual, seasonal, monthly and hourly wind variability.

2 COSMO numerical weather prediction model in Poland

Model COSMO version 5.01 is run at IMGW-NRI operationally four times per day using two nested domains at horizontal resolutions of 7 km and 2.8 km.

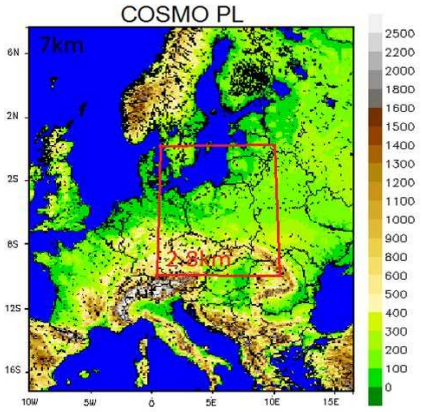

Figure 1: Cosmo model domain

Table 1: Operational setups of the COSMO-PL models.

Horizontal Grid Spacing [km]	7	2.8
Domain Size[grid points]	415 x 445	380 x 405
Forecast Range [h]	78	12
Inital Time of Model Runs[UTC]	00 06 12 18	1h frequency
Model Version Run	5.01	5.01
Model providing LBC date	ICON	COSMO PL7
LBC update interval [h]	3h	1h
Data Assimilation Scheme	Nudging	Nudging

COSMO model runs in a deterministic mode using initial (IC) and boundary (BC) conditions from ICON global model. Implemented in the COSMO observational data assimilation (DA) system is based on the nudging technique to improve forecast quality. DA allows for ingesting weather data measurements - as these carried out at SYNOP stations acquired from the WMO/GTS network.

The model is starting at 00, 06, 12, 18 UTC and produces 78 hour and 36 hour forecasts respectively at 7 and 2.8km resolutions.

3 Observational network

Our studies are based on the wind speed and wind direction data from the 2015 year, attained from two stations in Warsaw:

- Synoptic station **Okęcie(24h)** located on the south-west of Warsaw, within the Warszawa-Okecie airport.
- Climatological station **Bielany(6,12,18 h)** located in the northern part of Warsaw at the area of Institute of Meteorology and Water Management.

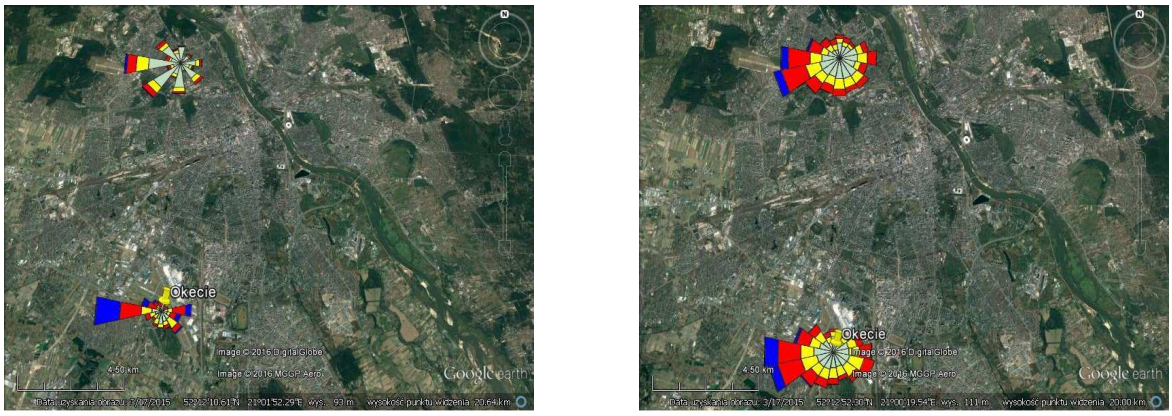

Figure 2: Wind roses in 2015 year at the Bielany and Okęcie stations (upper synop(left),lower model(right))

.

For our research we have collected data from all 24 hours of the synoptic station Okęcie and from three terms (06,12,18 h) of the Bielany climatological station from the whole 2015 year. Both stations are the multiannual network WMO stations. The station Warszawa Okęcie is located in the south-western parts of the city at the airport, while the station Bielany is situated in the northern part of the city near the Vistula River in the Institute of Meteorology and Water Management.

4 Data analysis

A wind rose is a concise and illustrative product showing wind speed and wind direction at a certain location. It provides information about the frequency of winds blowing at certain speed ranges from the particular direction, as well as its time percentage. For the selected locations we compare wind roses generated from NWP model with data from observational stations. Results are used both for the current meteorological analysis and for studies of a longer period of time. For current analysis WRPLOT View program was used [1].

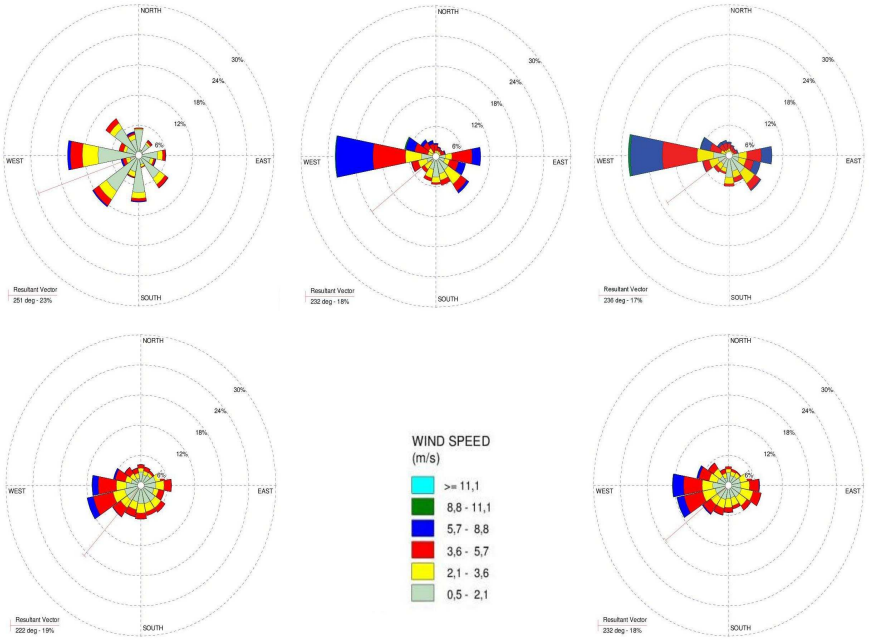

Figure 3: Wind roses: top - observation data: from left Bielany 3h, Okęcie 3h, Okęcie 24h; bottom - model: left Bielany, right Okęcie from 2015 year.

For direct comparison SYNOP observations from three terms (06,12,18 hours) at the Okęcie station have been selected. The predominant wind direction during the whole year for the station Okęcie is western. Surprisingly, we can observe very large convergence as for the wind direction and wind speed (Fig.3, Tab 2) calculated for the 3 hour and 24 hour averages, which shows how well is the data from 06,12,18 hours representative of a daily cycle.

A different distribution is observed at the station Bielany because it is located in different part of the city, between the residential area and forest, in a close proximity to the Vistula river, which significantly affects the distribution of winds in this area.

The winds have more scattered directions from north-west to south-east direction. COSMO model results show rather uniform wind speed and wind direction regardless of the location which indicates the need for implementing more detailed parametrization of urban effects.

Further analysis at the Bielany station (Tab 2) show smaller averaged annual wind speed (2.14 m/s) than at the Okęcie station (3.76 m/s) and over twice weaker winds speed dominating (Fig.4) in the class (0.5-2.1 m/s). By comparing model results with observational data we can see that at Okęcie station model wind speeds (2.94 m/s) are generally smaller than the observed one (3.57 m/s).

The class with the smallest wind speeds (0.5-2.1 m/s) increases by 30%, while the class with high wind speeds (5.7-8.8 m/s) significantly reduces by 10%. Whereas at the station Bielany situation is reversed, with higher wind speeds being observed in the model. The class of (3.6-5.7 m/s) increases of about 25%, while class of very weak winds (0.5-2.1 m/s) is reduced.

Table 2: Average wind speed and calm winds at Bielany and Okęcie for 2015 year

station	hours	calm wind	avg wind speed
Bielany obs.3h	1095	3.93	2.14
Okęcie obs.3h	1095	3.11	3.76
Okęcie obs.24h	8751	5.18	3.57
Bielany model	8724	0.11	2.79
Okęcie model	8724	0.16	2.94

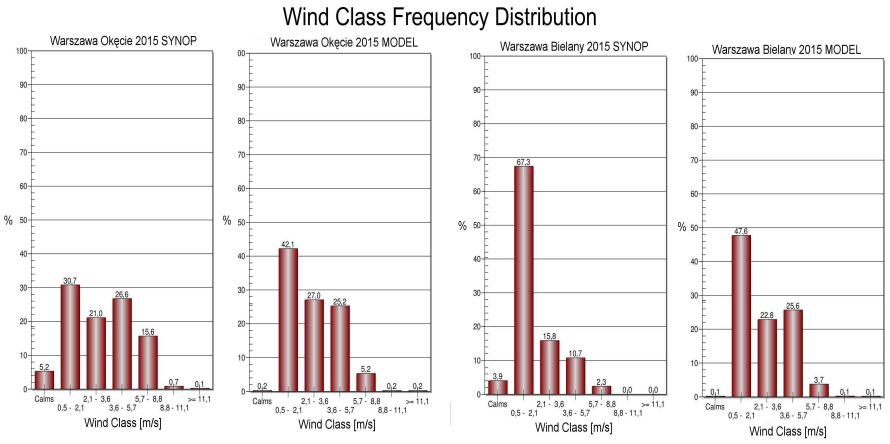

Figure 4: Wind class frequency distribution for 2015 year. From left: Okęcie synop/model, Bielany synop/-model.

A more detailed analysis was performed for the whole 2015 year (Fig. 5-8) and for individual months (Fig. 9-11) using hourly data (06,12,18 hours) from both meteorological stations and the COSMO model at 2.8km resolution . At both stations Bielany and Okęcie we can see for the observations a greater scatter in wind direction than in the data calculated by the model. (Fig 5-6).

Comparing the annually averaged wind speed (Fig. 5-10) we see that for Bielany, the wind speeds calculated from the model are higher than those observed at the station. At the Okęcie station situation is reversed, where wind speeds of observation are higher than those calculated by the model.

Comparing monthly averages for these hours we observe the highest wind speeds for 12 hours for both observations and model. The exception is the January at Okęcie with strong winds (over 4 m/s) throughout the day, where wind speeds of 18 hour is slightly higher than the wind speed at 12 hour.

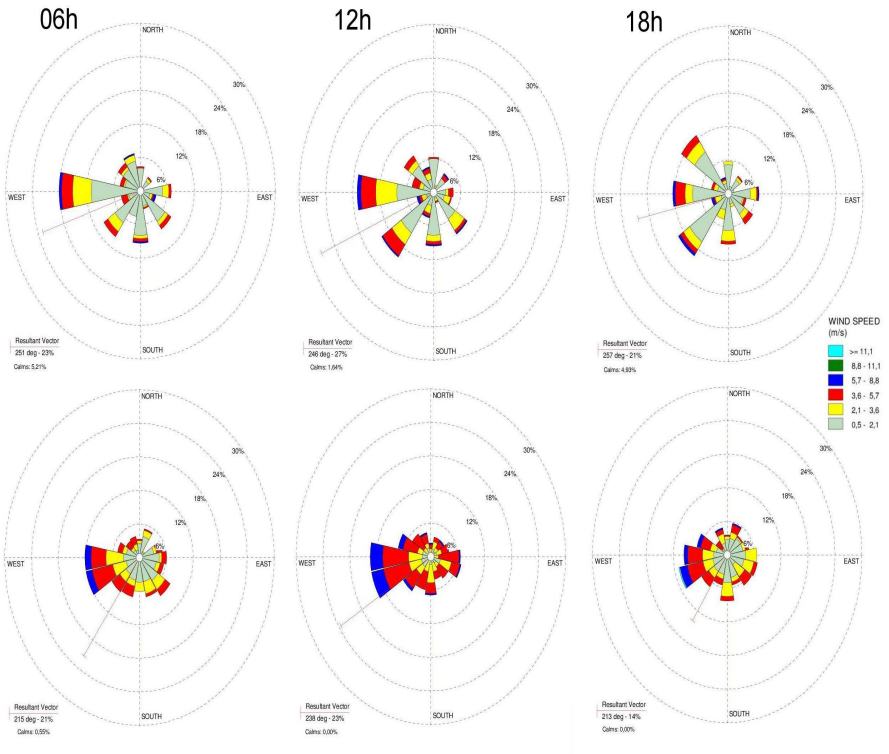

Figure 5: Hourly wind roses form 2015 year at Bielany station. From left: 06h 12h 18h, top - observation, bottom - model

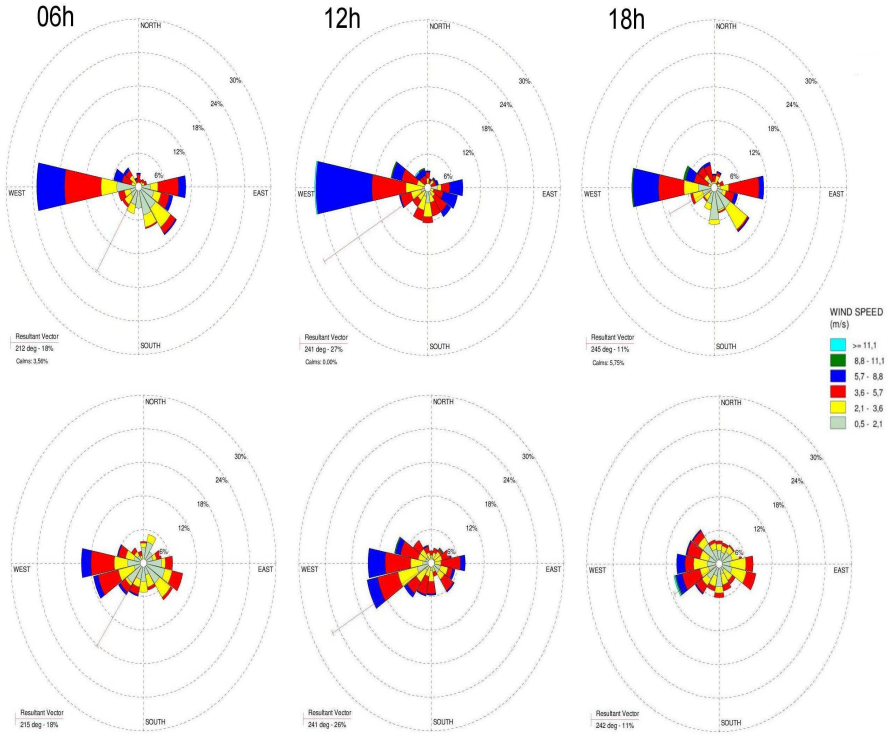

Figure 6: Hourly wind roses for 2015 year at Okęcie station. From left: 06h 12h 18h, top – synop, bottom - model

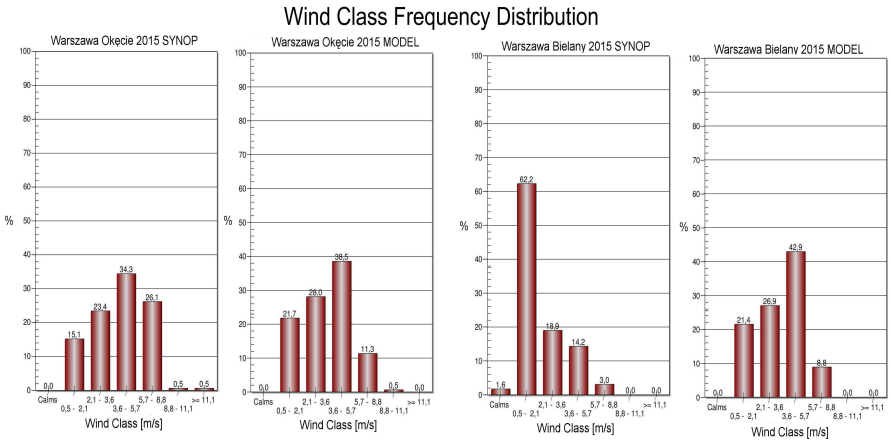

Figure 7: Wind class frequency distribution for 12 hour. From left: Okęcie synop/model, Bielany synop/-model

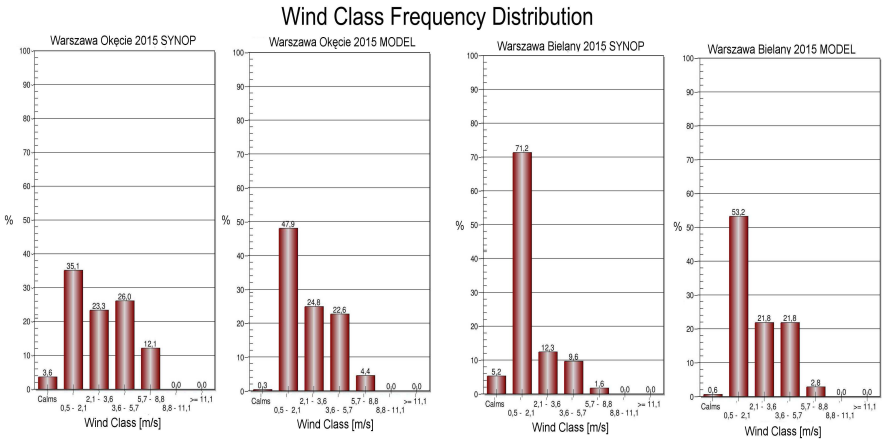

Figure 8: Wind class frequency distribution for 06 hour. From left: Okęcie synop/model, Bielany synop/-model

Monthly average wind speeds of 06 and 18 hour are similar in nature. In some months, we notice higher value of wind speeds for the 06 hours and the other for 18 hours. Therefore, to follow runs in individual wind speed classes only hours of 06 and 12 were selected (Fig 7,8). The general character of individual classes of wind frequency from the 12 hour is similar for Okęcie station and COSMO model.

The classes for higher wind speed (5.7-8.8 m/s) are significantly lower in the model (around 15%), whereas three lower wind speed classes from (0.5 to 5.7 m/s) are higher in the model (about 5% in each of these classes). At the station Bielany wind class frequency distribution from the 12 hour is completely different between model and the observations (Fig 7).

In model, the most numerous class is (3.6-5.7 m/s), which accounts for over 40% of cases, while at the station the most numerous class is (0.5-2,1 m/s) which accounts for over 60% of wind speed cases. The model for station Okęcie predicts for the classes (3.6-8.8 m/s) wind speeds lower than observed, while for the station Bielany the wind classes (2.1-8.8 m/s) have significantly higher speed than the observed one.

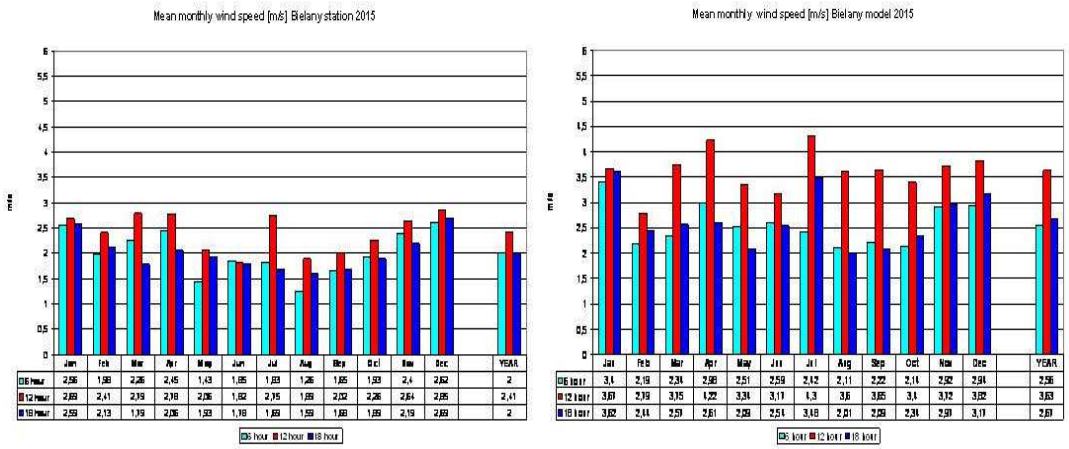

Figure 9: Mean monthly observation wind speed from 6,12,18 hours: Bielany,top/bottom station- model during the 2015 year

In the course of annual wind speeds from three terms (Fig. 9) at the station Warsaw-Bielany, the highest wind speeds we observe for the case of 12 hours, while the speed from hours 06 and 18 are smaller and have similar values to each other. The greatest differences in the course of the day between the hours of 12 and 06 and 18 are observed in July and the smallest in January, where the wind speeds during the day are very close to each other.

At the station Bielany we notice the lower wind speeds in the warm season from May to October (except for 12 hours in July), while higher wind speeds in the cold season from November to April. Comparing observational data with data from COSMO model we notice a higher wind speeds in model than observed at the station with a clearly dominant speeds from 12 hours.

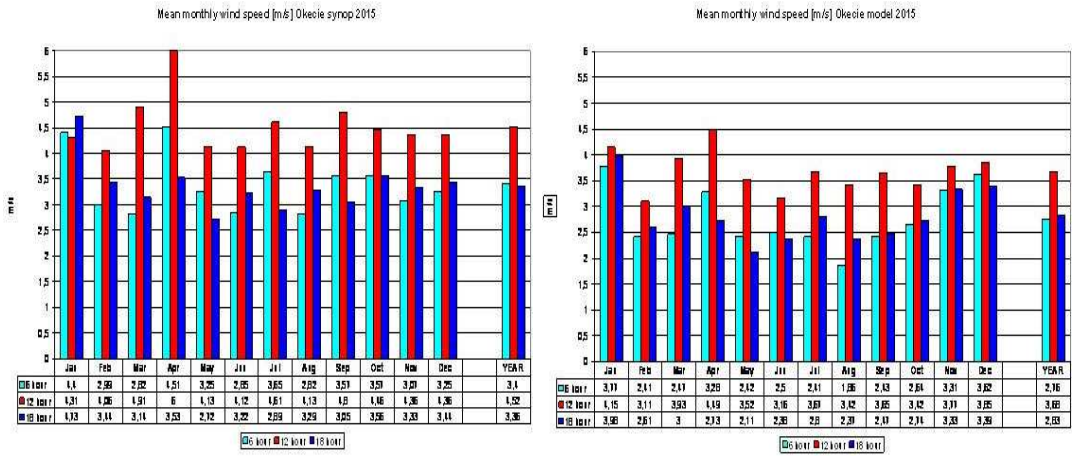

Figure 10: Mean monthly model wind speed from 6,12,18 hours: Okęcie, top/bottom synop-model during 2015 year

At the station Warsaw-Okęcie SYNOP data don't mark clearly the annual course (Fig.10) Wind speeds from 12 hour are dominant and their typical values for all months exceeds 4m/s. The exception is January where the difference in speeds between 06,12,18 hours are minimal and the highest wind speed is observed at 18 hour. The highest diurnal wind speed occurred in the month of April with a maximum 6 m/s for 12 hour case, and in January. The yearly velocity distribution in the 06,12,18 hours is different. The model forecasts in general underestimate the observations, which is well-preserved character of daily run.

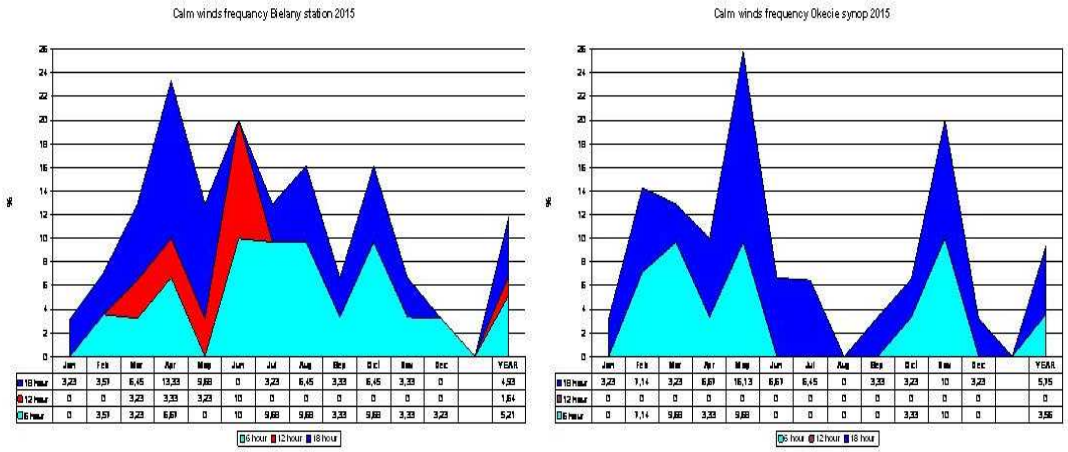

Figure 11: Calm wind frequency from 6,12,18 hours: top Bielany/bottom Okęcie in 2015 year

Figure 11 shows the calm wind frequency at the stations Bielany and Okęcie in selected hours of the day. At the station Okęcie of 12 hours there is no single case of calm wind in any month. For a few months in the summer and winter there was no calm wind at 06. In August there were no calm winds for any term during the day. Much more calm winds is observed at the station Bielany. In the months March and April calm wind is observed in all 06,12,18 hours. Minimum amount of calm winds we observe during the winter and maximum during the spring. In the COSMO model (tab.1,2) calm winds practically are not predicted very often (less than 1%) and are included in the lowest class of wind speed.

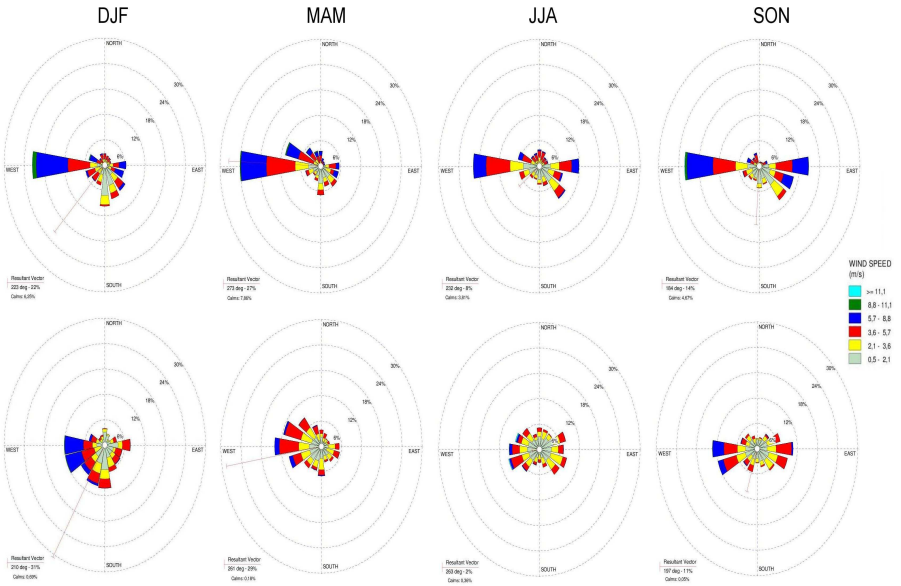

Figure 12: Seasonal wind roses: from December 2014 to November 2015 top, Okęcie synop , bottom Okęcie model

By analyzing the seasonal wind speed at the station Okęcie (Fig.12) we see the dominance of typical western circulation. However, in the individual seasons of 2015 there are observable differences in the flow direction. In the winter and spring (DJF, MAM) there are southern wind components, whereas at the end of summer (JJA) and autumn (SON) there are periods with a predominance of eastern and south-eastern winds. The model shows smaller wind speeds than the observed and a greater spread of wind directions.The best compatibility

Table 3: Seasonal average wind speed and calm wind,Okęcie 2015

Season	DJF	MAM	JJA	SON
avg. wind speed (m/s) synop	3.79	3.71	3.27	3.57
avg. wind speed (m/s) model	3.29	2.90	2.66	2.90
calm wind (%) synop	6.25	7.86	3.81	4.67
calm wind (%) model	0.69	0.18	0.36	0.05

of wind directions is during the autumn (SON).

In winter (DJF) directional dispersion in the model comes from the west to the south and for spring from the south-west to north-west. The highest amplitude of seasonal wind speeds is during winter (DJF) and the lowest in summer (JJA) (Tab.2). The model generated wind speed are for the whole season smaller than observed.

The lowest wind speed differences between observations and model are in winter (DJF) and the highest in spring (MAM). By analyzing calm winds, we see that in the model they are practically not existent. In the observation at the station Okęcie calm winds have higher values in winter (DJF) and spring (MAM) than in summer (JJA) and autumn (SON). In the spring, the amount of calm wind maximal and reaching almost 8%.

Summary

The aim of our work is to assess usability of model generated wind data for the idea of Smart Cities to exploit renewable energy of wind in urban areas, and possibly its effect on the boundary later dispersion and reduction of smog. Wind speed in Warsaw is sufficient for the installation of modern wind turbines for the production of renewable energy in the city. We compared two stations of which Okęcie can be treated as a suburban station while Bielany as a station in the city center. We observe a clear influence of the city on reducing wind speeds and changing wind directions related to the city infrastructure and the Vistula river. Three hours (06,12,18) were selected from the station Okęcie for comparison with the data at the station in Bielany. Data from 3 hour average were compared with 24 hour averages at the station Okęcie resulting in very small differences of wind speeds and directions.

Numerical model forecasts were also compared with observational data with the major difference being a lack of the calm winds in the model forecast. At the station Okęcie model wind directions are more scattered and have lower amplitude of wind speed, but distribution in each class shows a large similarity with observations. For the station Bielany model predicts much higher wind speed than the observed and numerical forecast did not reflect properly the wind direction. The further research will be continued with the direct implementation of urban effects within the TERRA-URB parametrization implemented the COSMO model.

References

[1] Lakes environmental software WRPLOT View *https://www.weblakes.com/products/wrplot/*

[2] Starosta K.,and Wyszogrodzki A.: Assessment of model generated wind energy potential In Poland. COSMO News Letter No.16

COMPARATIVE EVALUATION OF WEATHER FORECASTS FROM THE COSMO, ALARO AND ECMWF NUMERICAL MODELS FOR ROMANIAN TERRITORY

Rodica Claudia DUMITRACHE1, Simona TAŞCU1, Amalia IRIZA1, Mirela PIETRIŞI1,2, Mihaela BOGDAN1, Alexandra CRĂCIUN1, Bogdan Alexandru MACO1,3, Cosmin Dănuţ BARBU1, Tudor BĂLĂCESCU1, Simona BRICEAG1, Raluca IORDACHE1

1 National Meteorological Administration, Bucharest, Romania 2 University of Bucharest, Faculty of Physics 3 University of Bucharest, Faculty of Geography, Bucharest, Romania
rodica.dumitrache@meteoromania.ro

1 Introduction

The aim of this study is to assess the performance of the COSMO and ALARO limited are models and the ECMWF global model for Romanian territory.

For this purpose, we use the numerical forecasts of the COSMO model integrated for the operational domain covering the entire Romanian territory (figure 1) at 7 km horizontal resolution (201x177 grid points), with 40 vertical levels. The initial and lateral boundary conditions for the COSMO model are given by the ICON global model.

The ALARO limited area model is also integrated operationally for a domain covering the entire Romanian territory (figure 1) at 6.5 km horizontal resolution (240x240 grid points), with 60 vertical levels. The initial and lateral boundary conditions for the COSMO model are taken from the ARPEGE global model.

For the present comparative evaluation we also take into account the numerical weather forecasts of the ECMWF model available for the Romanian territory (interpolated at roughly 10 km horizontal resolution).

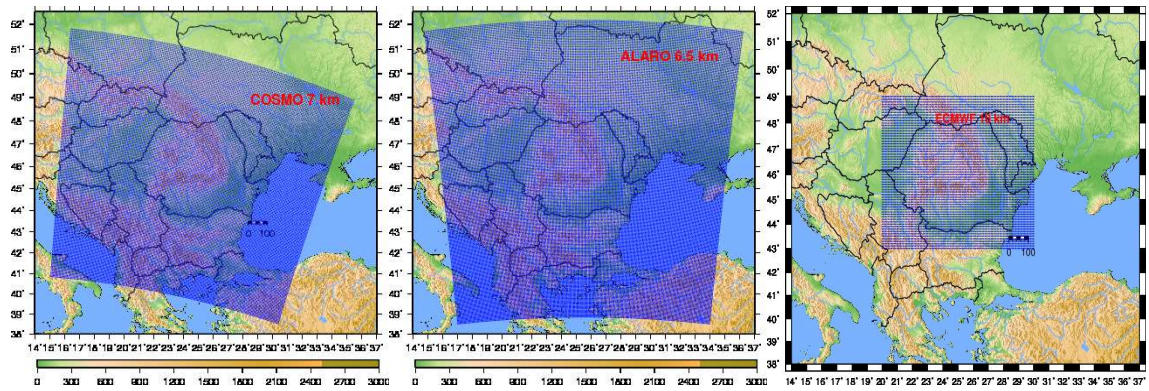

(a) (b) (c)

Figure 1: Integration domains and associated topography height of COSMO (a), ALARO (b) and ECMWF (c) for Romanian territory.

2 Case Study

The performance of the 00UTC runs from the three models for Romanian territory was analyzed for three consecutive seasons: DJF (December 2015 – February 2016), MAM (March 2016 – May 2016) and JJA (June 2016 – August 2016). The verification of the models was performed taking into account all SYNOP observations available for Romanian territory (160 stations). All available SYNOP observations (in BUFR format), as well as numerical weather forecasts and corresponding topography files for each of the three models (in GRIB1 format) were uploaded into the VERSUS system, which was used for this comparative evaluation. Statistical scores were computed for 2 meter temperature, pressure reduced to mean sea level, 10 meter wind speed and 6-hour cumulated precipitation.

2 meter temperature, pressure reduced to mean sea level and 10 meter wind speed were ingested into the VERSUS system using the nearest grid point optimized method (1), while mean values on a 15 km radius method (6) was used to ingest cumulated precipitation. ME (mean error) and RMSE (root mean squared error) were computed for continuous parameters, along with scatter plots. Dichotomic scores POD (probability of detection), FAR (false alarm rate), PC and ETS (equitable threat score) were used to evaluate hours precipitation for different thresholds, along with performance diagrams.

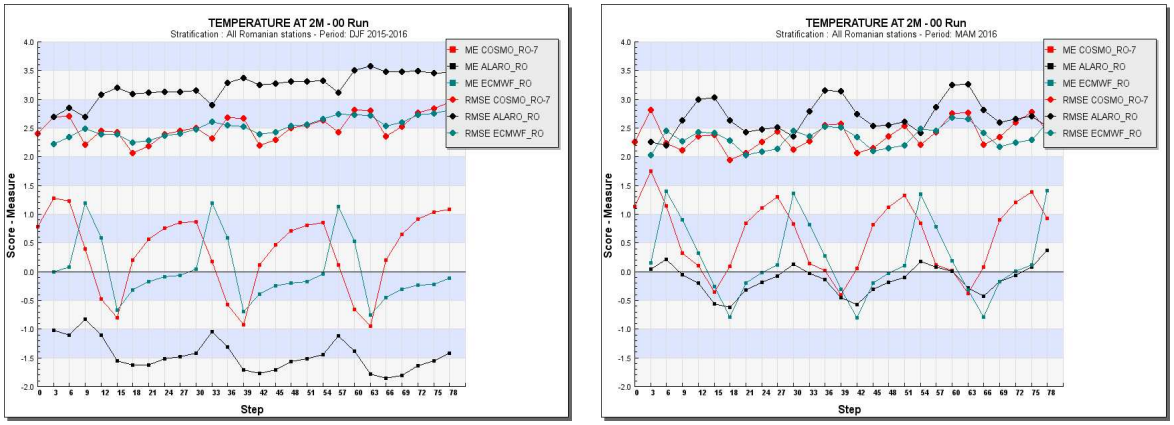

(a)

(b)

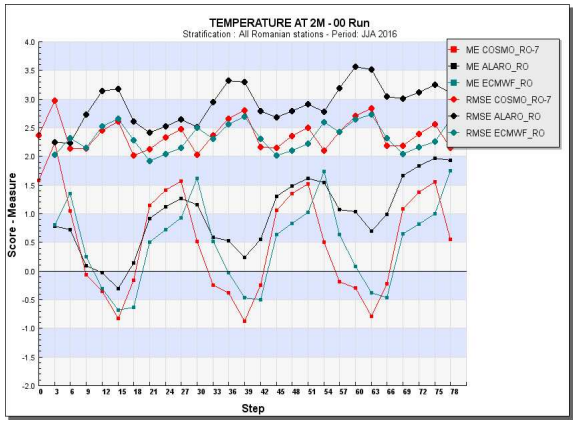

(c)

Figure 2: 2 meter air temperature, ME and RMSE - COSMO-7km (red); ALARO (black) and ECMWF (blue): DJF (a), MAM (b) and JJA (c)

For 2 meter temperature (figure 2), both the COSMO and the ECMWF models display the same sistematic behaviour for all three analyzed seasons. The general tendency of the two models is to underestimate forecasted values during the day, while overestimating during night time, comparred to observations. While ME values for COSMO and ECMWF (for Romanian territory) are comparable, lower RMSE values from the COSMO model for the entire period of interest suggest a better performance than the ECMWF model in forecasting this parameter.

The ALARO model integrated for Romanian territory strongly underestimates this parameter during winter and overestimates its values during summer. Although the ALARO model displays the smallest ME values from the MAM season, higher RMSE values suggest a larger amplitude of errors compared to the other two models.

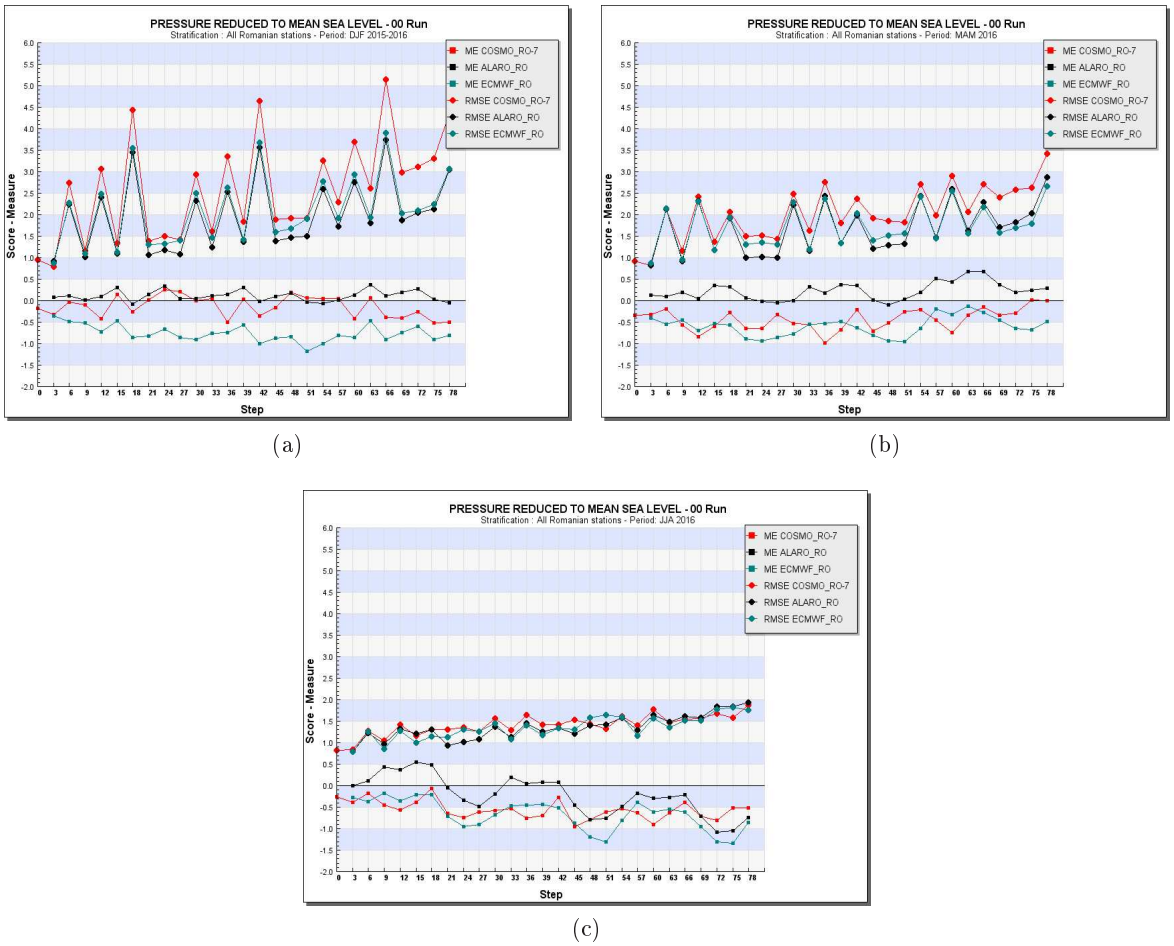

(a) (b)

(c)

Figure 3: Pressure reduced to mean sea level, ME and RMSE - COSMO-7km (red); ALARO (black) and ECMWF (blue): DJF (a), MAM (b) and JJA (c)

ME values for mean sea level pressure from the COSMO model show again a sistematic behaviour for all three seasons (figure 3). The general tendency of the model is to underestimate the values for this parameter with up to 1 hPa compared to the synoptic observations, especially for the MAM and JJA seaons. Slightly reduced errors can be observed for the DJF season. However, for most of the DJF and MAM seasons, the COSMO model integrated for Romanian territory displays the highest amplitude of errors, quantifiable by the larger RMSE values, compared to the other two numerical models.

The genral tendency of the ALARO model integrated for Romanian territory is to slightly overestimate the forecasted values for mean sea level pressure during winter (DJF) and spring (MAM), while for the summer period (JJA), the tendency of the model is to underestimate this parameter after the first day, compared to the observations. RMSE values for the DJF, MAM and JJA seasons suggest that the ALARO model has a smaller amplitude of errors compared to the COSMO and ECMWF models. Finally, the ECMWF model displays the overall tendency of underestimating the values for pressure reduced to mean sea level, and has the largest mean errors from the three models.

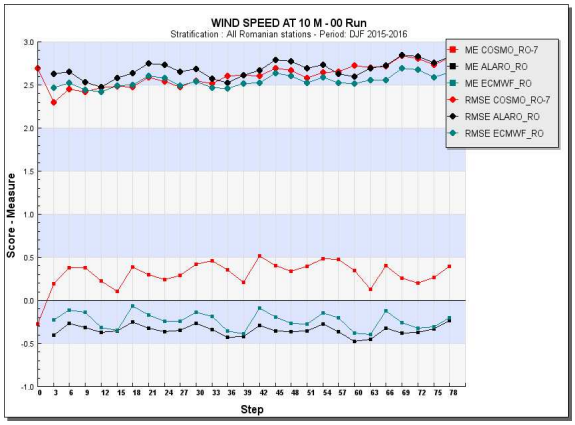

(a)

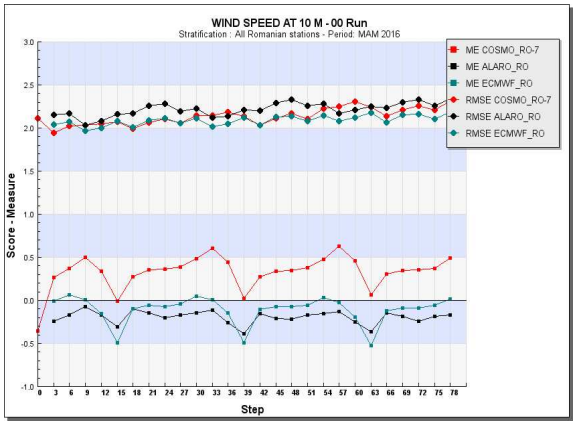

(b)

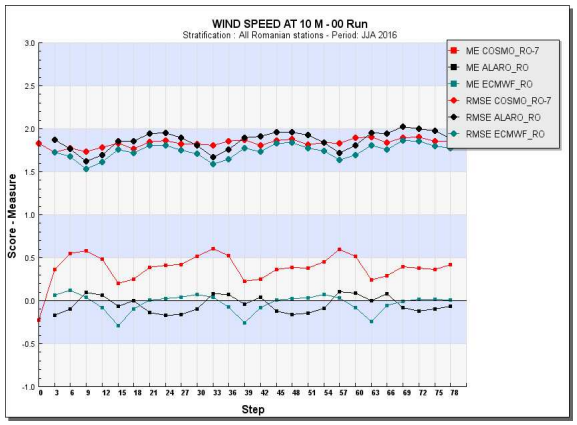

(c)

Figure 4: 10 meter wind speed, ME and RMSE - COSMO-7km (red); ALARO (black) and ECMWF (blue): DJF (a), MAM (b) and JJA (c)

All three models display high accuracy in forecasting 10 meter wind speed, with mean errors between -0.5 m/s and 0.5 m/s and a reduced amplitude of errors, especially for the summer period (figure 4). Comparable values for ME and RMSE are obtained for the entire forecast period, suggesting that the models offer a good estimation of this parameter even with up to 78 hours anticipation. Similar to the forecast for 2 meter temperatures and pressure reduced to mean sea level, the COSMO model displays a sistematic behaviour for all seasons; except for the first step (+0), 10 meter wind speed values are always slightly overestimated compared to the observations (with up to 0.5 m/s), for the entire period of interest. Although ME values for the ALARO and ECMWF models seem slightly lower, especially for the JJA season, these two models do no exhibit the same sistematic behaviour for all the seasons, as is the case of the COSMO model.

The limited area models COSMO and ALARO integrated for Romanian territory display a higher accuracy in forecasting 6-hour cumulated precipitation than the global ECMWF model. The scores presented in figures 5-7 were computed for 6-hour cumulated precipitation over 0.2 mm. The highest probability of detection for the two limited area models are obtained for the winter season (up to 0.8 - 0.9), while the lowest results for POD are obtained during the convective season (JJA). This suggests that roughly 3/4 of the observed rain events are estimated correctly for the winter season (figure 5), while the ratio can drop up to 2/4 for the summer, with a slight worsening during the last hours of forecast, for all three seasons. For the spring season and especially for the summer season, it can be noticed that the COSMO and ALARO models integrated for Romanian territory display a better ability in capturing the rain events during the day, while POD drops during night time (figures 6 and 7). This behaviour is also noticeable for the ECMWF model, during the convective season (JJA).

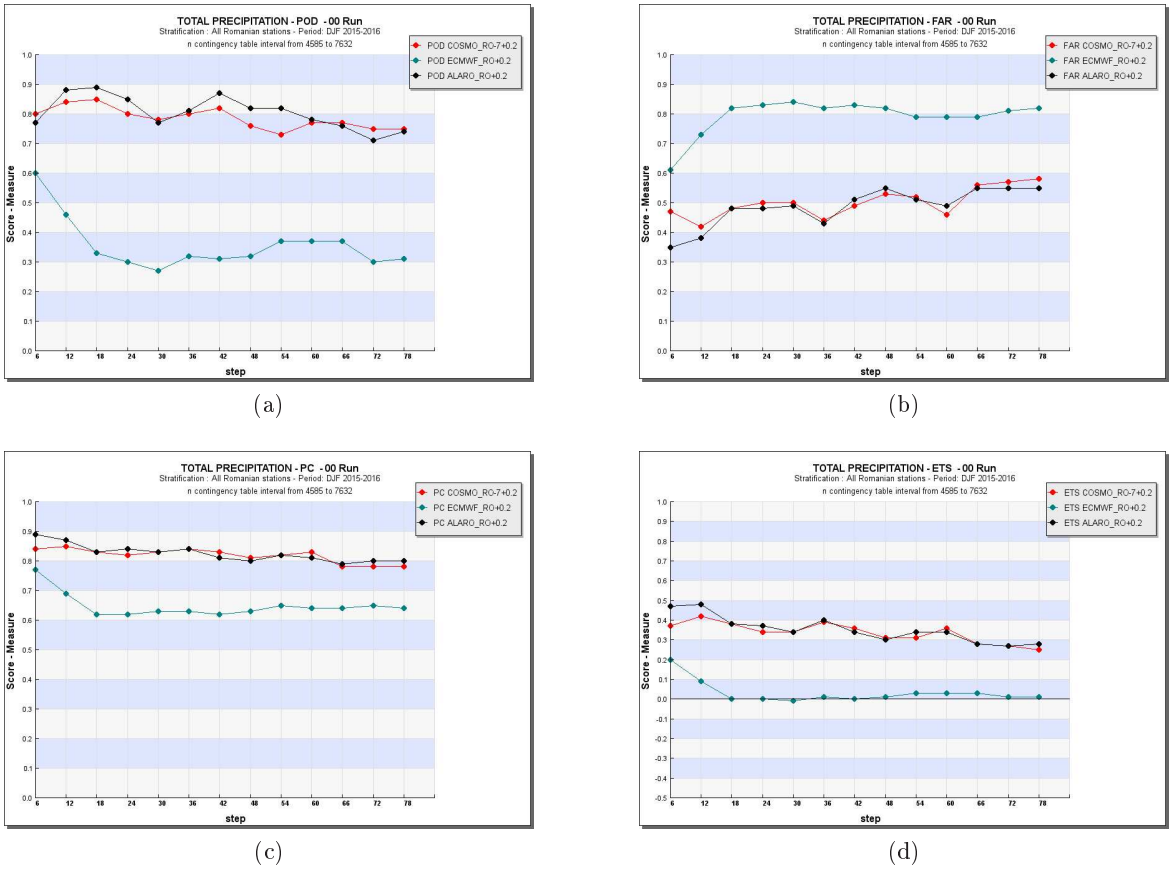

Figure 5: 6-hour cumulated precipitation for DJF - COSMO-7km (red); ALARO (black) and ECMWF (blue): POD (a), FAR (b), PC (c) and ETS (d)

The FAR results computed for ECMWF forecasts suggest that the model tends to overpredict the occurence of rain for all three seasons, while for the COSMO and ALARO models in roughly up to 1/3 – 1/2 of the of the forecast rain events, rain was not observed. Similar to the case of POD, the FAR score also shows a slight worsening in the forecast of this parameter for the last anticipations. Finally, the ETS values for the COSMO and ALARO models suggest that roughly half of the observed rain events were forecasted correctly.

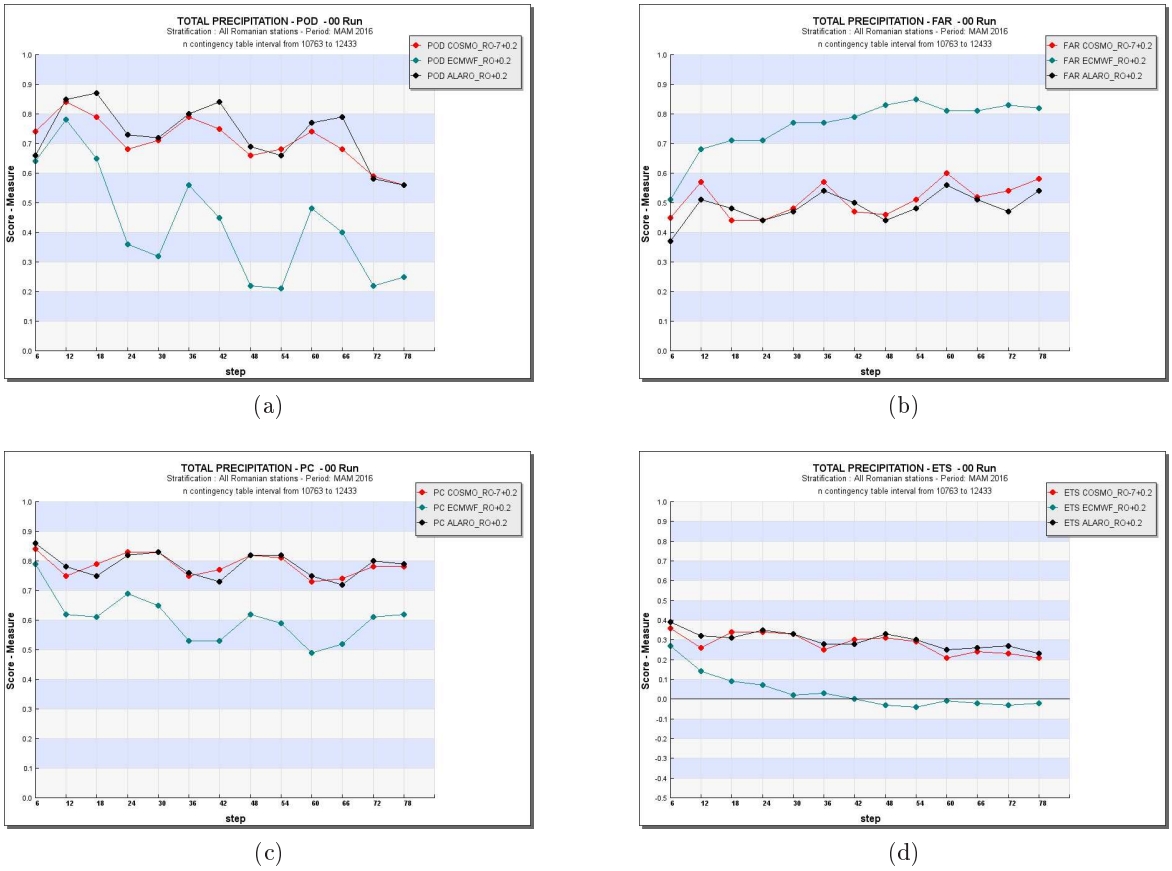

Figure 6: 6-hour cumulated precipitation for MAM - COSMO-7km (red); ALARO (black) and ECMWF (blue): POD (a), FAR (b), PC (c) and ETS (d)

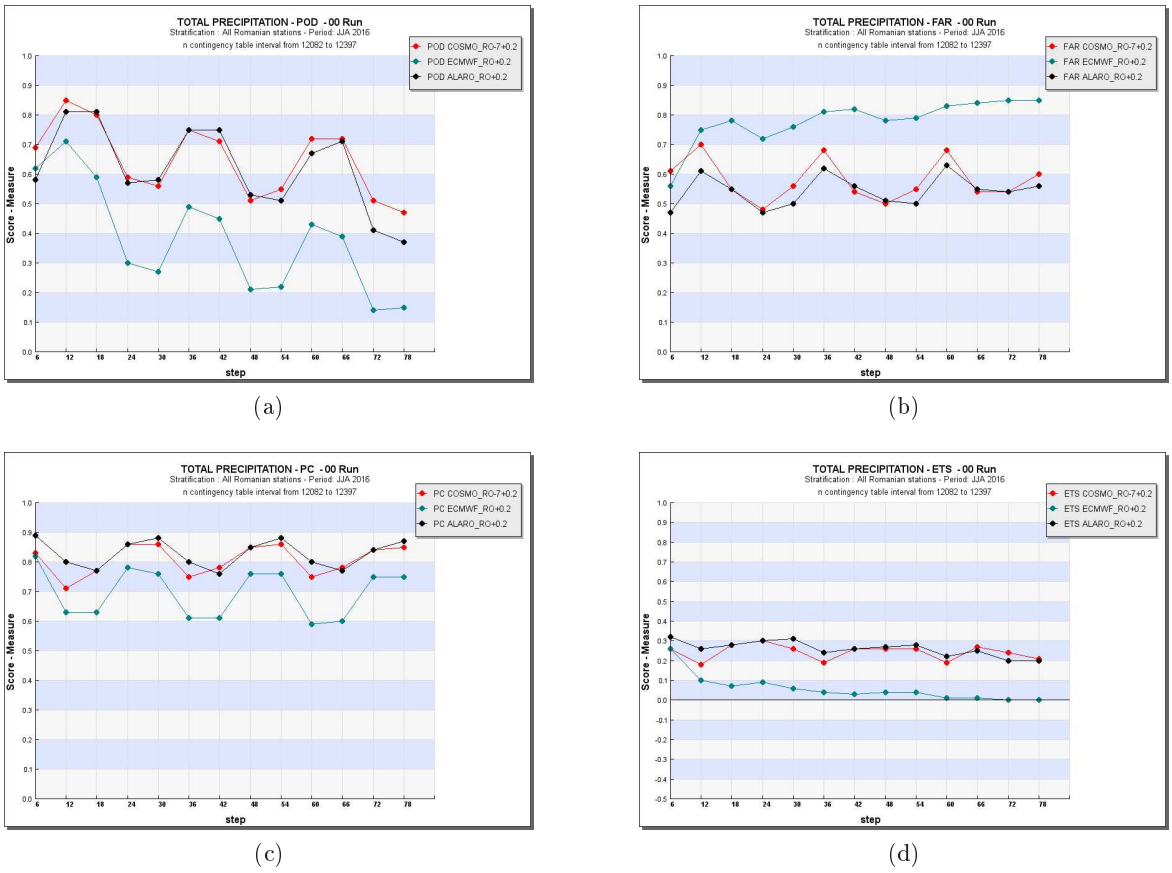

Figure 7: 6-hour cumulated precipitation for JJA - COSMO-7km (red); ALARO (black) and ECMWF (blue): POD (a), FAR (b), PC (c) and ETS (d)

References

[1] http://www2.cosmo-model.org/content/model/documentation/core/default.htm

[2] http://www.cnrm-game-meteo.fr/aladin/

[3] http://www.rclace.eu/

[4] http://www.rclace.eu/

[5] http://www.meteoam.it/

Running the COSMO model on unusual hardware architectures - part 2

Davide Cesari

Arpae-SIMC, Bologna, Italy

1 Introduction

In a previous paper [1] it was shown how it is possible to run a complex numerical code such as the COSMO model on a small device designed for a completely different purpose: a home satellite TV receiver running the Linux operating system. In this paper a similar test is performed on an even smaller and cheaper –though more powerful– device, the Raspberry Pi single-board computer.

2 Characteristics of the device

The Raspberry Pi is a general-purpose computer on a very small board, measuring only $85x56mm^2$. It has a processor belonging to the ARM architecture, the one used by most of the smartphones today available on the market. The device used for the test is the Raspberry Pi 3 model B, the latest and most powerful model available at the moment, having a quad-core Broadcom processor with a GPU (Graphical Processing Unit) and 1 GB of memory. The board is also equipped, among the others, with wired and wireless network links, USB connections, video and audio output and SD card mass storage, which make it qualitatively comparable to an usual desktop or server computer.

This board is very popular among hobbyists for projects integrating external sensors and active devices with a powerful and easily programmable CPU, however, thanks to its computing power, it is perfectly suitable for traditional "number-crunching" applications. The official website is `http://www.raspberrypi.org`.

The most common operating system for the Raspberry Pi is a full version of Debian GNU-Linux, which, together with 1 GB of RAM, makes the question "is it possible to run the COSMO model on it?" superfluous.

The price of this board is around 35 Euros, thus making it one of the cheapest devices capable of running the COSMO model.

3 Preparation of the sequential test

In order to make a clean comparison with the results previously obtained, the same version of the compiler and of the COSMO model used in the previous tests, GNU gfortran 4.9.2 and COSMO version 5.00 respectively, have been used for the present work.

As shown in the previous paper on this subject, a viable way to produce an executable for such an architecture is *cross-compiling* on a desktop computer, i.e. generating the binary executable for the device on a computer having a different architecture and a special version of the compiler. This avoids the trouble of installing the complete compiler suite on the device and allows also to circumvent a possible unsuitability of the device to perform a full optimising compilation, e.g. due to lack of memory.

For compiling a sequential version of the COSMO code, the same instructions indicated in the previous paper have been followed. Due to the use of an ARM instead of a MIPS architecture on the device, the cross-compiler installation commands wee modified accordingly:

```
dpkg --add-architecture armhf
apt-get update
apt-get install crossbuild-essential-armhf
apt-get install gfortran-arm-linux-gnueabihf
```

After this step, the commands for compiling, linking and generating libraries for the Raspberry Pi are the usual commands such as `gfortran`, `gcc`, `ar`, etc. prefixed by the string `arm-linux-gnueabihf-`.

Also the setup of the sequential (single process, non-MPI) test case was the same used in the previous paper: a 3-dimensional idealised case of a rising warm bubble, implemented into COSMO by Ulrich Blahak [2], on a $21 \times 21 \times 40$ point grid with an horizontal step of 2km and a time step of 12s.

4 Performing the test

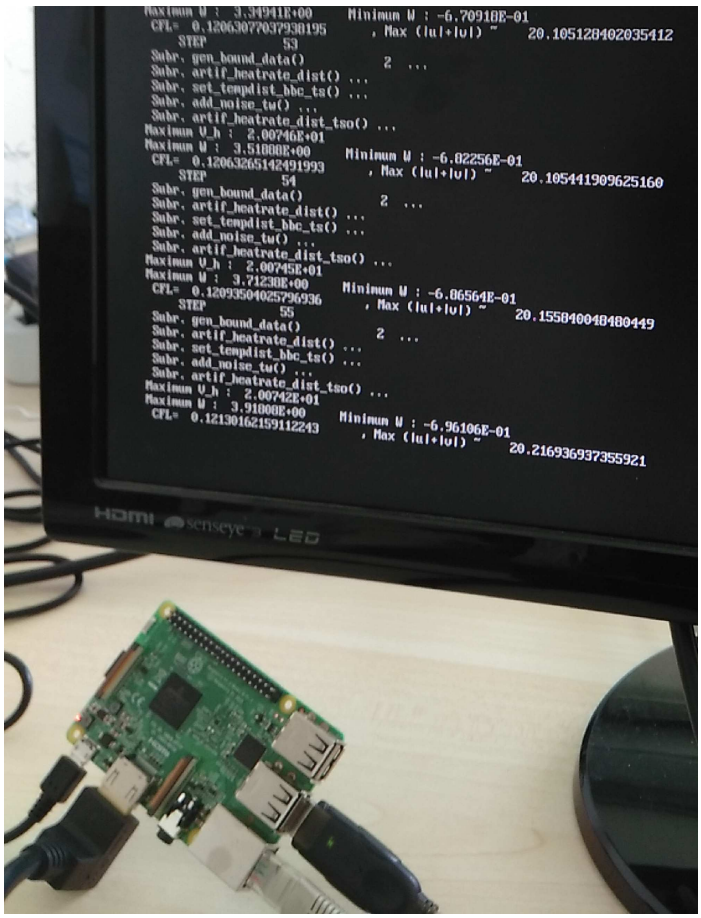

Figure 1: The Raspberry Pi connected to a huge screen, caught while running the COSMO model.

The test is performed by simply copying the executable and the namelists to the device connected to the network and by logging in to the device and running the COSMO model as usual. Since the Raspberry Pi, unlike the devices used in the previous paper, can have a console on the connected keyboard and monitor, the process of running the model on it can have a more exciting visual feedback on the screen as shown in the photo at figure 1.

5 Results of the sequential test

Table 1 summarises the results of the sequential test in terms of total wall-clock time required for one hour of forecast with the configuration described, as reported in the YUTIMING file. The table shows also the results obtained on the previously tested MIPS platforms as well as the results on a state of the art HPC computing node (price ≈2000 EUR) using a single processing core.

These results show that the Raspberry Pi lies logarithmically in the middle between the weak MIPS TV receiver tested in the previous work and the HPC computing node.

Platform	wall clock time (s)
Raspberry Pi 3B	139
Gigablue 800 UE	1111
Gigablue 800 SEplus	28649
HPC computing node	12

Table 1: Summary of the sequential tests performed, including the old results.

6 Parallel MPI tests

Since the Raspberry Pi has a processor with multiple computing cores and much more memory than the MIPS devices previously tested, a second and more interesting test with an MPI version of the code has been set up. This parallel version of the code can simultaneously run on two or more of the available cores and the parallel processes communicate through the shared memory.

The compilation of the MPI version of the COSMO model has also been performed as cross-compilation on an external host with a different architecture, this time generating a dynamical executable linking shared libraries. However, since the MPI software involves not just linking with additional libraries, but also a more complex compilation and runtime environment, the cross-compilation process did not work as cleanly as before, but it required some dirty tricks and hand corrections, so it is not described here.

Anyway, thanks to the relatively powerful hardware for the device under test and the availability of a complete operating system on it, it is perfectly feasible to compile the COSMO model with MPI support directly on the device, in the same way as it is usually compiled on a workstation or HPC login node.

Initially, the same test introduced before has been performed with the MPI version of the COSMO model, using from one to all of the four computing cores available. For comparison, the same test has been performed on the HPC node already used for the sequential test, using all the available processors/cores. The results are shown in table 2.

Platform	MPI processes and geometry	wall clock time (s)
Raspberry Pi 3B	1×1	138
Raspberry Pi 3B	1×2	98
Raspberry Pi 3B	1×3	89
Raspberry Pi 3B	1×4	92
Raspberry Pi 3B	2×2	99
HPC computing node	1×12	5.4

Table 2: Summary of the first parallel test performed.

This proves that the COSMO model with the setup described above shows some parallel scaling capability on the Raspberry Pi, but it can hardly profit of the third computing core, not counting the fourth.

It can also be noted that the MPI version does not introduce extra overhead with respect to the sequential (so-called "dummy MPI") version of the code, when run as a single MPI process.

Due to the partially unsatisfactory scaling, a more challenging setup has been prepared, by doubling the number of grid points on either direction ($41 \times 41 \times 40$) while keeping the same space resolution and time step. The temperature disturbance ("bubble") has been kept of the same size in the center of the enlarged domain.

The scaling results of this second experiment are shown in table 3.

Finally, another test, after further doubling the domain size on x and y directions, has been performed, whose results are shown in table 4.

These two tests show that with a more suitable domain size, the strong scaling of the COSMO code on the device under test is significantly better and all the four cores can give a positive contribution to the reduction of the time to solution.

Platform	MPI processes and geometry	wall clock time (s)
Raspberry Pi 3B	1×1	677
Raspberry Pi 3B	1×2	388
Raspberry Pi 3B	1×3	321
Raspberry Pi 3B	1×4	308
Raspberry Pi 3B	2×2	323
HPC computing node	1×12	15

Table 3: Summary of the second parallel test performed.

Platform	MPI processes and geometry	wall clock time (s)
Raspberry Pi 3B	1×1	3012
Raspberry Pi 3B	1×2	1713
Raspberry Pi 3B	1×3	1341
Raspberry Pi 3B	1×4	1230
HPC computing node	1×12	48

Table 4: Summary of the third parallel test performed.

7 Conclusions

Unlike the results presented in the previous paper, these results show that the architecture under test can compete with an HPC architecture in pure terms of performance per money and performance per watt.

Indeed the ratio between the figures for Raspberry Pi and a state of the art HPC node can be estimated to be approximately 1/60 for the price, 1/40 for the power consumption and 1/25 for the performance (of course referred to the COSMO model), thus with a little advantage for the Raspberry. Of course, due to the huge number of nodes that would be required, it is not feasible to employ such an architecture as it is for real parallel computing, but these results show that it is worth exploring this direction.

References

[1] Cesari, D., 2016: Running the COSMO model on unusual hardware architectures. COSMO Newsletter no.16 *Available online http://cosmo-model.org/content/model/documentation/newsLetters/newsLetter16/default.htm*

[2] Blahak, U., 2015: Simulating idealized cases with the COSMO-model. *Available online http://www.cosmo-model.org/content/model/documentation/core/artif_ docu.pdf*, 48pp.

Experiments with stochastic perturbation of physical tendencies in COSMO-Ru2-EPS

DMITRY ALFEROV AND ELENA ASTAKHOVA

Hydrometcenter of Russia, Roshydromet, Moscow, Russia

Abstract

The experiments with the scheme of stochastic perturbation of physical tendencies (SPPT) were carried out using the COSMO-Ru2-EPS ensemble prediction system. Several SPPT settings were tested. Both case studies and probabilistic verifications of forecast monthly series were performed.

It was found that SPPT could be useful for precipitation forecasts improving the description of the rain location and start, increasing the ensemble spread in the areas of uncertain forecasts, and slightly improving the probabilistic scores.

SPPT does not add value to 2-m temperature forecasts but results in a better description of the 2-m temperature distribution. It is possible to improve the skill of temperature forecasts by varying the SPPT settings.

1 Introduction

Ensemble forecasting is a common method for predicting the future state of the atmosphere and the probability of this state. The well-known problem of ensembles is their insufficient spread.

The RMSE of prognostic realizations with respect to the ensemble mean (the ensemble spread) and the RMSE of the ensemble mean with respect to observations should demonstrate a similar growth with forecast lead-time, but it is often not so.

To increase the ensemble spread and to get its adequate growth in time, it is necessary to allow for forecast uncertainties following not only from errors in our knowledge of the initial atmospheric state (that is, from possible errors in initial and lateral boundary conditions) but also from the model imperfections as well as from errors in surface boundary conditions.

In this paper, we examine how the implementation of the scheme of stochastic perturbation of physical tendencies (SPPT) to the COSMO-Ru2-EPS system affected the ensemble spread and performance.

2 Experiment setup

In our experiments, we used the COSMO-Ru2-EPS system that had been previously developed within the framework of the CORSO Priority project (Rivin, Rozinkina, 2011). The system provided a dynamical downscaling of COSMO-S14-EPS, the Italian ensemble prediction system for the Sochi-2014 Olympics.

In turn, COSMO-S14-EPS was a clone of COSMO-LEPS (Montani et al., 2011) moved to the Sochi region. The systems are sketched in Fig. 1 and described in detail in (Montani et al., 2013, 2014).

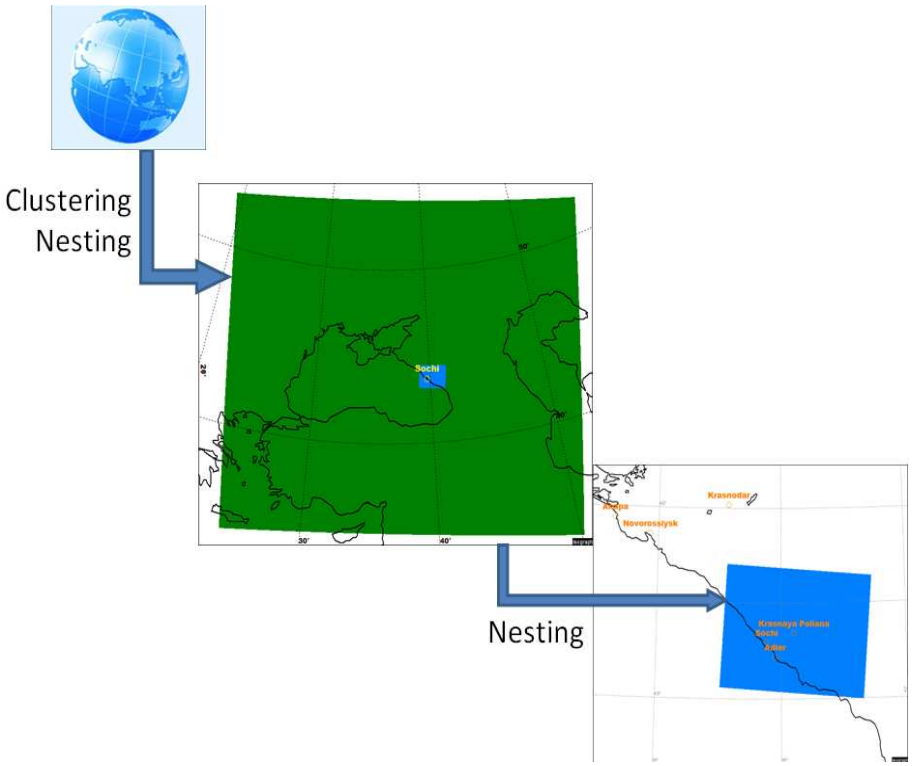

Figure 1: Ensemble nesting for Sochi. The integration domains for COSMO-S14-EPS and COSMO-Ru2-EPS are colored blue.

Both COSMO-S14-EPS and COSMO-Ru2-EPS ran operationally during the Olympic Games 2014 providing probabilistic products to Sochi forecasters. All observations and forecasts issued during the Olympics are stored in a special TIGGE-LAM styled archive (Astakhova et al., 2016) thus facilitating further research.

In this study we extracted the operational COSMO-Ru2-EPS forecasts for February 2014 starting at 00 and 12 UTC from the archive and used them as a reference experiment hereafter referred to as noSPPT. Some details of the operational runs are summarized in Table 1.

Table 1: COSMO-Ru2-EPS settings for the operational Olympic runs (**noSPPT** experiment)

Model	COSMO model version 4.22
Forecast area	Sochi region (see Fig. 1)
Grid step	2.2 km
Number of levels	50
Initial& boundary conditions	Taken from COSMO-S14-EPS (COSMO-LEP relocated to the Sochi region; see Fig.1)
Membership	10
Forecast length	48h
Output time step	1h
Physical perturbations	No perturbations (no SPPT scheme included)

After the Olympic Games, additional experiments were carried out with COSMO-Ru2-EPS with the aim to test the SPPT scheme and to assess its effect on the forecast spread and skill. The model resolution, the integration domain, the forecast length, the ensemble size, as well as initial and boundary conditions were the same as in the reference experiment **noSPPT**.The period from February 1 to February 28, 2014 was considered.

The SPPT scheme (Buizza et al., 1999) has been implemented to the COSMO model v.5.1. However, due to the courtesy of L. Torrisi and C. Schraff, who provided the necessary software, we could start the experiments prior to the official release of version 5.1. Therefore, the first experiments with the SPPT scheme at Roshydromet were performed with version 5.0 of the COSMO model complemented by some additional modules. Later, after the SPPT scheme had been introduced to the official COSMO code and model version 5.1 had been released, we changed to this version in our experiments. Have in mind that version 5.1 didn't differ much from version 5.0 with additional modules.

There are several parameters in the SPPT scheme that govern the perturbation size and their spatiotemporal correlations. A full description of SPPT settings can be found in COSMO User's Guide (Schaettler et al., 2014). The goal of our experiments was not only to test SPPT with its recommended parameters but also to understand to which degree the variations of these parameters (the SPPT setting) influence the results. We tried the following parameters, defining several aspects of random number field generation:

- the random number coarse grid distances **dlat_rn** and **dlon_rn**;
- the type of distribution of random numbers **lgauss_rn**;
- the standard deviation of the Gaussian distribution of random numbers **stdv_rn**;
- the upper limit imposed to the absolute value of random numbers **range_rn**;
- the parameter showing whether the random numbers are interpolated in space **lhorint_rn** and time **ltimeint_rn**;
- number of random number patterns with different correlation scales **npattern_rn**;
- time increment for drawing new random number field **hinc_rn**.

We also tried to vary the parameter **itype_qxpert_rn**, showing which hydrometeor tendencies are perturbed, and the parameter **itype_qxlim_rn**, determining the type of reduction/removal of the perturbation in case of negative or supersaturated values of specific water vapor content or negative other water-content related characteristics.

The list of experiments and the corresponding SPPT settings are given in Fig.2. COSMO model v. 5.1 was used in all experiments except for the experiment **SPPTtest** which was run with COSMO model v.5.0. Note that the reference experiment **noSPPT** was based on COSMO model v.4.22.

Both case studies and verification of monthly series of forecasts were carried out. The results are presented in the next sections.

3 Case studies

The main attention was given to the ability of COSMO-Ru2-EPS to predict precipitation and 2-m temperature over the mountain area. Two cases were analyzed, both from the list of interesting events prepared by the Olympic forecasters and recommended for thorough analysis (see Astakhova et al., 2016). The results of experiments **SPPTtest** and **noSPPT** were considered.

<table>
<tr><th rowspan="2">Perturbed parameters</th><th colspan="7">Experiment name and SPPT settings</th></tr>
<tr><th>noSPPT</th><th>SPPTtest</th><th>SPPTphys</th><th>SPPTintphys</th><th>SPPT_W</th><th>SPPT_W +phys</th><th>SPPT_W +intphys</th></tr>
<tr><td>lgauss_rn</td><td rowspan="11">N/A</td><td colspan="6">.TRUE.
(Gaussian distribution)</td></tr>
<tr><td>hinc_rn
(hours)</td><td colspan="6">6</td></tr>
<tr><td>dlat_rn, dlon_rn
(degrees)</td><td colspan="6">5</td></tr>
<tr><td>stdv_rn</td><td colspan="3">0.4</td><td colspan="3">1.0</td></tr>
<tr><td>range_rn</td><td colspan="3">0.8</td><td colspan="3">0.9</td></tr>
<tr><td>lhorint_rn</td><td colspan="2">.FALSE.
(no interpolation of perturbations)</td><td>.TRUE.
(interpolated perturbations)</td><td>.FALSE.
(no interpolation of perturbations)</td><td colspan="2">.TRUE.
(interpolated perturbations)</td></tr>
<tr><td>ltimeint_rn</td></tr>
<tr><td>itype_qxpert_rn</td><td>0
(q^v only)</td><td colspan="5">2
(q^v, q^c, q^i, q^r, q^s, q^g)</td></tr>
<tr><td>itype_qxlim_rn</td><td>0
(no limitations imposed)</td><td colspan="2">1
(do not perturb tt T- and tt q^v tendencies if new q^v are negative or supersaturated)</td><td>0
(no limitations imposed)</td><td colspan="2">1
(do not perturb tt T- and tt q^v tendencies if new q^v are negative or supersaturated)</td></tr>
<tr><td>npattern_rn</td><td colspan="6">1</td></tr>
</table>

Figure 2: The list of experiments and the corresponding SPPT settings.

The first case was the tropospheric Foehn event on February 7, 2014. It was characterized by higher than usual 2-m temperature with very weak diurnal variations, low humidity, and east and southeast winds at 1500–2300 m. The rise of atmospheric temperature at about 1500 m above the sea level was poorly predicted by most models from many countries participating in the FROST-2014 project (the WWRP RDP/FDP project devoted to the Sochi Olympics, Kiktev et al., 2014, 2017).

The ensemble spread fields obtained for this case with and without SPPT were compared. The interesting thing found in the difference of the spread fields was that it depended on orography. Figure 3 demonstrates the difference of 2-m temperature spread in 30-h forecasts with and without SPPT (experiments **SPPTtest** and **noSPPT**) (top) and the model orography (bottom). The correlation of the fields is obvious.

The maximum increase of the spread due to SPPT introduction was found over high mountains, the spread over low areas (including sea) was also big. Meanwhile, at middle altitudes, SPPT somewhere even decreased the ensemble spread.

The strongest increase in the ensemble spread at high altitudes along with the fact of poor temperature forecasts above 1500 m in this case can be considered as a positive effect of SPPT introduction (areas of higher spread coincided with the areas of less skillful forecast).

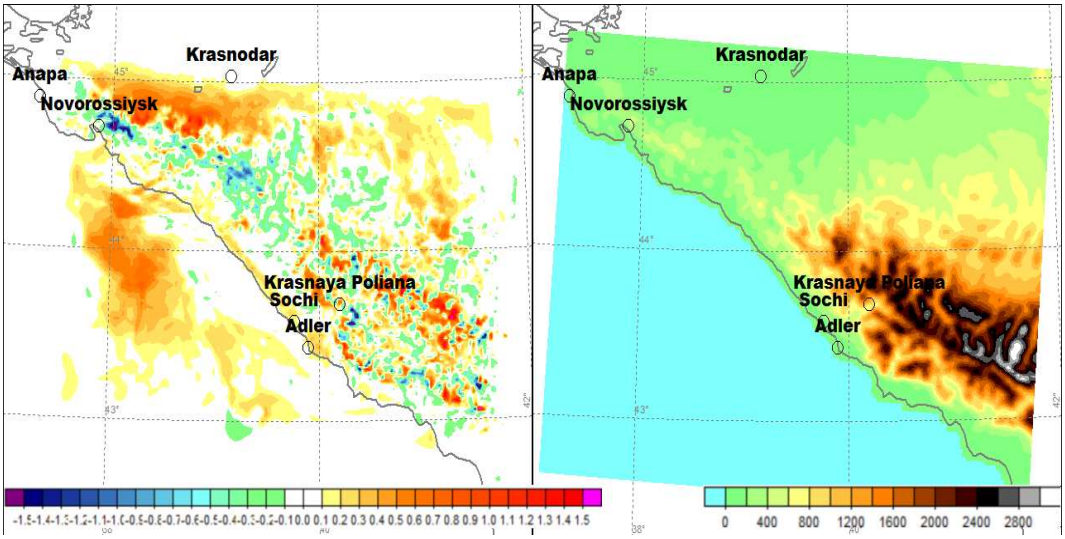

Figure 3: Left panel: The difference of 2-m temperature ensemble spread in experiments with and without SPPT (**SPPTtest** minus **noSPPT**). 30-h forecast starting at 00 UTC on February 6, 2014. Right panel: model orography.

We also considered a heavy precipitation event on February 18, 2014. The fields of predicted probabilities of the rain occurrence (rain exceeding 0.1 mm in 3 h) and of intense precipitation (more than 10 mm of rain in 3 h) in experiments **SPPTtest** and **noSPPT** were compared to METEOSAT data (not shown).

The comparison demonstrated that the system with SPPT was more skillful in predicting the time when it started raining. Also less false heavy rain areas and more actual peaks were predicted in the **SPPTtest** experiment. However, the location of maximum precipitation was better described in the **noSPPT** experiment.

4 Verification results

We used the results of **SPPTtest** and **noSPPT** experiments as well as the results of five more experiments with various SPPT settings (see Fig.2) in the verification exercise. The considered period was 1–28 February 2014. The forecasts were issued twice a day starting from 00 and 12 UTC analyses; the forecast length was 48 hours. No separation by the initial forecast time was made, thus we used a series of 56 forecasts in computations.

The verification was performed for three meteorological fields: 3-hour total precipitation sum (R_{sum}), 2-m air temperature (T_{2m}) and 10-m wind speed. The following three ensemble forecast scores were considered: the Brier score (BS), the Brier skill score (BSS) and the area under the ROC curve (ROCA). (It's worth reminding here that the perfect scores are BS=0, BSS=1, ROCA=1).

The verification was made against observations of 31 meteorological stations in the Sochi region (see Figure.

4). R-based utilities developed and kindly provided by A. Muravev were applied.

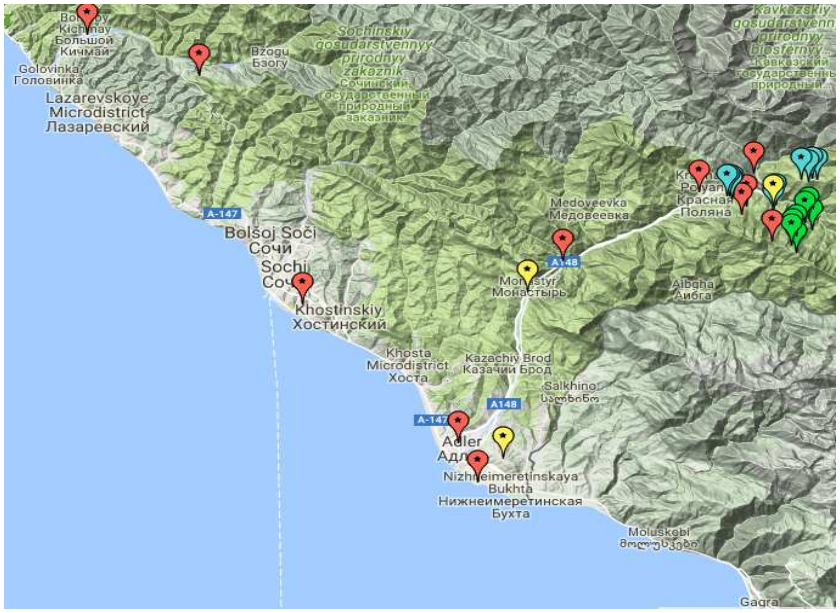

Figure 4: Stations used for verification (see the FROST-2014 project website http://frost2014.meteoinfo.ru/ for details)

.

The resulting scores are presented in Figures.5-6.

It was nice to see that the introduction of SPPT did not result in the precipitation forecast degradation. Figure 5 demonstrates BS, BSS and ROCA as functions of forecast lead-time for the events "3-h precipitation is greater than 0.1 mm/3h, 1 mm/3h, and 5 mm/3h" for all experiments listed in Fig 2.

The scores for different experiments are very close. However, for higher thresholds ($R_{sum} > 1$ mm/3h and $R_{sum} > 5$ mm/3h) the **SPPTtest** experiment gives the best results. Note that intense precipitation (R_sum > 5 mm/3h) is predicted badly in all experiments (BSS is low, even below zero for some lead-times). It is probably related to insufficient statistics, such events were rather rare during the period considered.

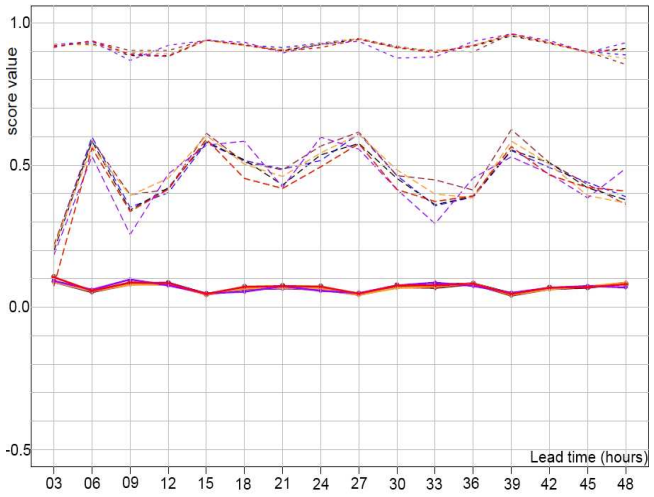

(a)

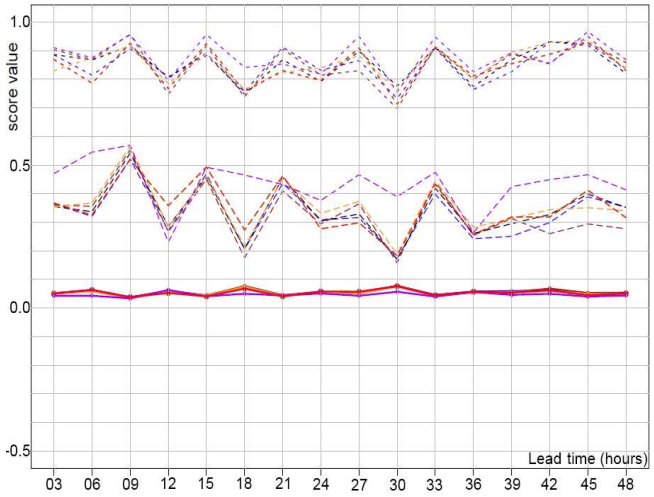

(b)

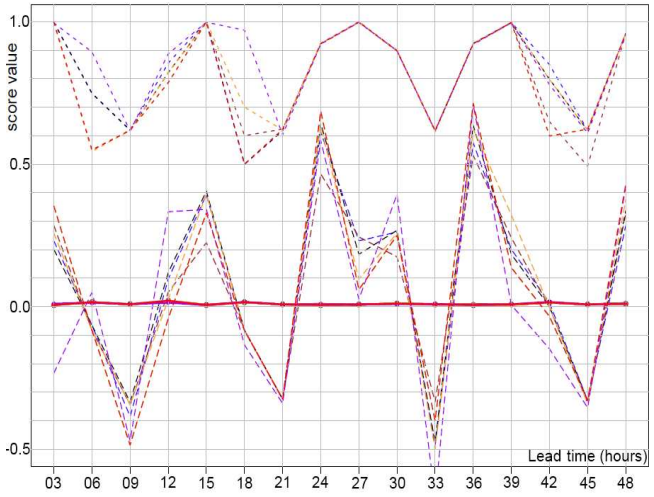

(c)

Figure 5: Verification scores as functions of forecast lead-time for the events "3-h precipitation (R_{sum}) is greater than 0.1 mm/3h (a) , 1 mm/3h (b) , and 5 mm/3h (c) " for all experiments listed in Fig.2. Solid line: BS, long-dashed line: BSS, dashed line: ROCA. Red lines: noSPPT, purple: SPPTtest, orange: SPPTphys, black: SPPTintphys, green: SPPT_W, brown: SPPT_W+phys, blue: SPPT_W+intphys. February 2014; 31 stations.

The results were not so encouraging for 2-m temperature forecasts. Figure 6 demonstrates the verification scores for the two events "2-m temperature is above 0°C" and "2-m temperature is above 5°C". For the first event, BS and ROCA are very similar for all experiments, while BSS is slightly better for **noSPPT**. However, for the second event (panel b), the situation changes significantly. The scores range much between the experiments and the great diversity of results gives a chance to analyze the effect of different SPPT settings. The experiment **noSPPT** is clearly the best for all lead times. In contrast to precipitation forecasts, the 2-m temperature predictions are the worst for **SPPTtest** (violet in the plots). Analyzing the curves, we can conclude that interpolation of perturbed values in space and time did not affect the scores noticeably. Most likely it is associated with too coarse perturbation grid (compared to the model grid) used in the experiments. Also only a small effect followed from varying itype_qxlim_rn def, which defined the type of reduction/removal of the perturbation in case of negative or supersaturated values of water vapor content or negative other water-content related characteristics. The scores additionally suggest that not only specific water vapor tendencies but all hydrometeor tendencies should be perturbed.

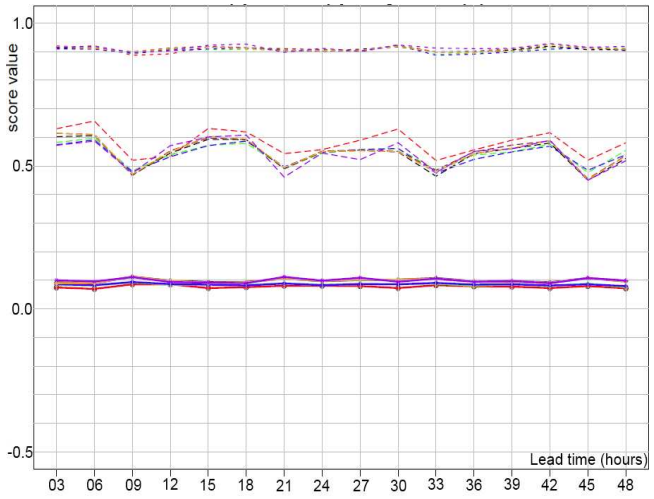

(a)

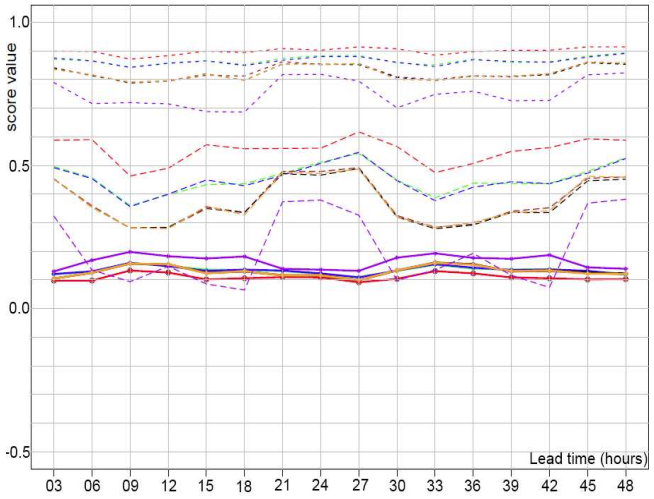

(b)

Figure 6: Verification scores as functions of forecast lead-time for the events "2-m temperature is above 0°C" (a) and "2-m temperature is above 5°C" (b) for all experiments listed in Fig.2. Solid line: BS, long-dashed line: BSS, dashed line: ROCA. Red lines: noSPPT, purple: SPPTtest, orange: SPPTphys, black: SPPTintphys, green: SPPT_W, brown: SPPT_W+phys, blue: SPPT_W+intphys. February 2014; 31 stations.

The importance of perturbing all humidity tendencies is confirmed by the skill of ensemble mean forecasts obtained in different experiments. In Fig. 7 the mean error (ME), the mean absolute error (MAE) and the root-mean-square error (RMSE) of 2-m temperature ensemble mean forecasts at Krasnaya Poliana station are presented as functions of lead-time for all the experiments.

Here we again see the prevalence of **noSPPT** experiment in RMSE, MAE, and ME. **SPPTtest** experiment, in which only specific water vapor tendencies were perturbed, gave the largest errors. Perturbing all hydrometeor tendencies helps to improve the scores.

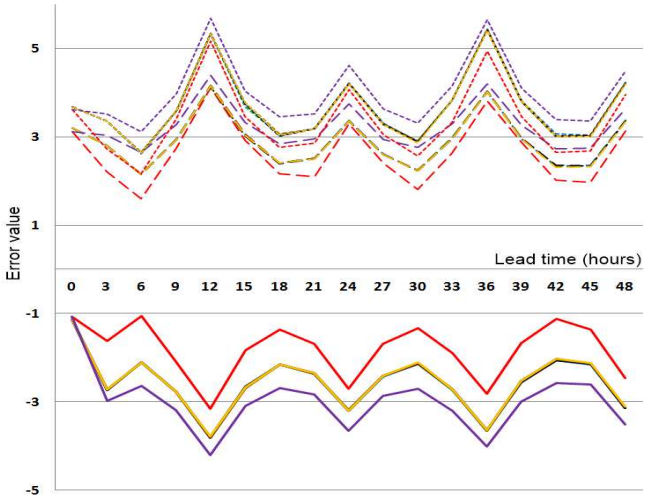

Figure 7: Error graphs for T_{2m} ensemble mean forecasts at Krasnaya Poliana station. Solid line: mean error, long-dashed: mean absolute error, dashed: RMS error. Red lines: noSPPT, purple: SPPTtest, orange: SPPT-phys, black: SPPT_intphys, green: SPPT_W, brown: SPPT_W+phys, blue: SPPT_W+intphys. February 2014.

To complete the analysis, we decided to examine distributions of observed and predicted temperatures. Figure 8 demonstrates the temperature distribution histograms at Krasnaya Poliana for experiments **noSPPT** and **SPPTtest** (the distributions for experiments with other SPPT settings were alike). The eyeball analysis shows that SPPT seems to make the representation of temperature distribution more accurate.

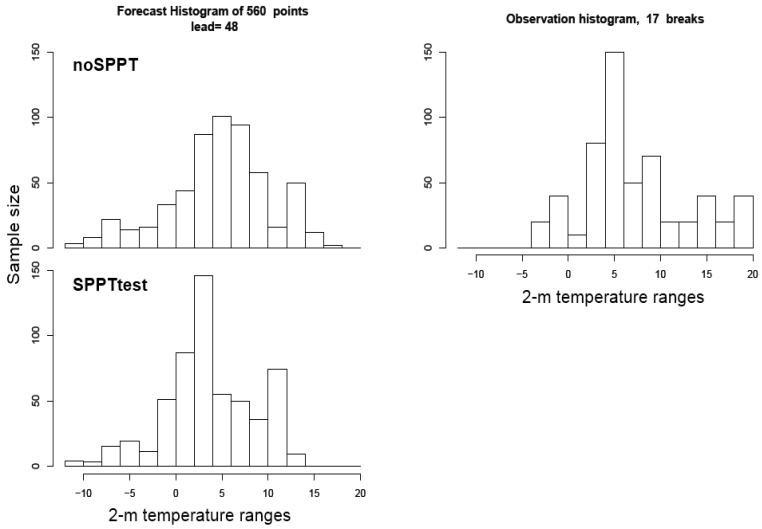

Figure 8: Comparison of T_{2m} distribution histograms for **noSPPT** and **SPPTtest** 48-h forecasts and for observations. February 2014.

Wind speed forecast scores were rather poor both with and without SPPT. SPPT did not make significant difference. Therefore we do not present them here.

5 Conclusions

The experiments with the scheme of stochastic perturbation of physical tendencies (SPPT) were performed using the COSMO-Ru2-EPS ensemble prediction system. The initial and boundary conditions for the runs were provided by COSMO-S14-EPS, the Italian ensemble prediction system developed within the framework of the WWRP FDP/RDP project FROST-2014. The period 1–28 February 2014 was considered. The operational forecasts issued during the Sochi Olympic Games 2014 were used as a reference. Several SPPT settings were tested. Both case studies and probabilistic verifications of forecast series were performed.

Case studies demonstrated that SPPT could be useful for precipitation forecasts improving the description of the rain location and start. The analysis of 2-m temperature predictions in the tropospheric Foehn case revealed the correlation between the T_{2m} ensemble spread and the model orography. Also the coincidence between high-spread areas and the areas of less skillful forecast was found.

The probabilistic verification was performed for the monthly series of COSMO-Ru2-EPS forecasts (56 in total). Some positive effect of using SPPT was found for precipitation forecasts, especially for the event "3-h precipitation is greater than 1 mm". Variations in the SPPT settings did not influence the results much. As for the 2-m temperature forecasts, SPPT does not improve their skill. The verification scores showed rather large difference between experiments with various SPPT settings. Judging by Brier score, the Brier skill score and the area under the ROC curve, the experiment without SPPT gave the best temperature forecasts.

At the same time, the eyeball analysis shows that introduction of SPPT makes the predicted temperature distribution more realistic. Therefore, SPPT did not add value to temperature forecasts, but can sometimes improve the representation of distribution. It is possible to improve the T_{2m} forecast by varying the SPPT settings. For example, perturbing all hydrometeor tendencies in most cases leads to better results than perturbing only specific water content tendency. Also increasing the range of standard deviation for the Gaussian distribution of random numbers and using the higher upper limit imposed to the absolute value of random numbers positively contributed to the results.

Acknowledgments

The authors are grateful to Lucio Torrisi and Christoph Schraff for providing additional SPPT modules for COSMO model version 5.0, Anatoly Muravev for verification software, and Andrea Montani for providing initial-boundary conditions. The study was made within the COTEKINO and SPRED COSMO priority projects.

References

[1] Astakhova, E., A. Montani, D. Kiktev, A. Smirnov: 2016: COSMO-based ensemble forecasting for Sochi-2014 Olympics: archiving the results. COSMO Newsletter, No. 16, **P.40-45**. Available online at *http* : *//cosmo − model.org/content/model/documentation/newsLetters/newsLetter*16/*cnl*16$_0$6*.pdf*

[2] Buizza, R., Miller M., Palmer T., 1999: Stochastic representation of model uncertainties in the ECMWF Ensemble Prediction System. Q. J. R. Met. Soc. ,vol. 125, **P.2887–2908**.

[3] Kiktev, D. B., Astakhova E. D., Zaripov R. B., Murav'ev A. V., Smirnov A. V, and Tsyrulnikov M.D., 2015: FROST-2014 project and meteorological support of the Sochi-2014 Olympics. Russian meteorology and hydrology, vol.40, iss.8, **P.504-512**. DOI 10.3103/S1068373915080051.

[4] Kiktev, D., P. Joe, G. Isaac, A. Montani, I. Frogner, P. Nurmi, B. Bica, J. Milbrandt, M. Tsyrulnikov, E. Astakhova, A. Bundel, S. Belair, M. Pyle, A. Muravyev, G. Rivin, I. Rozinkina, T. Paccagnella, Y. Wang, J. Reid, T. Nipen, and K. Ahn, 2017: FROST-2014: The Sochi Winter Olympics International Project. Bull. Amer. Meteor. Soc. DOI:10.1175/BAMS-D-15-00307.1, in press.

[5] Montani, A., Cesari D., Marsigli C., Paccagnella T., 2011: Seven years of activity in the field of mesoscale ensemble forecasting by the COSMO-LEPS system: main achievements and open challenges. Tellus, 63A, **P.605-624**. DOI: 10.1111/j.1600-0870.2010.00499.x

[6] Montani, A., C. Marsigli, and T. Paccagnella, 2013: Development of a COSMO-based limited-area ensemble system for the 2014 Winter Olympic Games. COSMO Newsletter, No. 13,**P.93–99**. Available online at *http* : *//cosmo − model.org/content/model/documentation/newsLetters/newsLetter*13/*cnl*13$_1$2*.pdf*.

[7] Montani, A., D. Alferov, E. Astakhova, C. Marsigli, and T. Paccagnella, 2014: Ensemble forecasting for Sochi-2014 Olympics: the COSMO-based ensemble prediction systems. COSMO Newsletter, No. 14, **P.88–94**. Available online at *http : //cosmo − model.org/content/model/documentation/newsLetters/newsLetter*14/*cnl*14$_1$0.*pdf*.

[8] Rivin G. and Rozinkina I., 2011: Priority Project "CORSO": Consolidation of Operation and Research results for the Sochi Olympic Games. Available online at *http : //cosmo − model.org/content/tasks/pastProjects/corso/default.htm*

[9] Schaettler U., Doms G., Schraff C. A., 2014: Description of the Nonhydrostatic Regional COSMO-Model. Part VII: User's Guide. Offenbach. November 2014. **P.211**.

List of COSMO Newsletters and Technical Reports

(available for download from the COSMO Website: `www.cosmo-model.org`)

COSMO Newsletters

No. 1: February 2001.

No. 2: February 2002.

No. 3: February 2003.

No. 4: February 2004.

No. 5: April 2005.

No. 6: July 2006; Proceedings from the COSMO General Meeting 2005.

No. 7: May 2008; Proceedings from the COSMO General Meeting 2006.

No. 8: August 2008; Proceedings from the COSMO General Meeting 2007.

No. 9: December 2008; Proceedings from the COSMO General Meeting 2008.

No.10: January 2010; Proceedings from the COSMO General Meeting 2009.

No.11: February 2011; Proceedings from the COSMO General Meeting 2010.

No.12: March 2012; Proceedings from the COSMO General Meeting 2011.

No.13: April 2013; Proceedings from the COSMO General Meeting 2012.

No.14: April 2014; Proceedings from the COSMO General Meeting 2013.

No.15: July 2015; Proceedings from the COSMO General Meeting 2014.

No.16: June 2016; Proceedings from the COSMO General Meeting 2015.

No.17: July 2017; Proceedings from the COSMO General Meeting 2016.

COSMO Technical Reports

No. 1: Dmitrii Mironov and Matthias Raschendorfer (2001):
Evaluation of Empirical Parameters of the New LM Surface-Layer Parameterization Scheme. Results from Numerical Experiments Including the Soil Moisture Analysis.

No. 2: Reinhold Schrodin and Erdmann Heise (2001):
The Multi-Layer Version of the DWD Soil Model TERRA_LM.

No. 3: Günther Doms (2001):
A Scheme for Monotonic Numerical Diffusion in the LM.

No. 4: Hans-Joachim Herzog, Ursula Schubert, Gerd Vogel, Adelheid Fiedler and Roswitha Kirchner (2002):
LLM — the High-Resolving Nonhydrostatic Simulation Model in the DWD-Project LITFASS.
Part I: Modelling Technique and Simulation Method.

No. 5: Jean-Marie Bettems (2002):
EUCOS Impact Study Using the Limited-Area Non-Hydrostatic NWP Model in Operational Use at MeteoSwiss.

No. 6: Heinz-Werner Bitzer and Jürgen Steppeler (2004):
Description of the Z-Coordinate Dynamical Core of LM.

No. 7: Hans-Joachim Herzog, Almut Gassmann (2005):
Lorenz- and Charney-Phillips vertical grid experimentation using a compressible nonhydrostatic toy-model relevant to the fast-mode part of the 'Lokal-Modell'

No. 8: Chiara Marsigli, Andrea Montani, Tiziana Paccagnella, Davide Sacchetti, André Walser, Marco Arpagaus, Thomas Schumann (2005):
Evaluation of the Performance of the COSMO-LEPS System

No. 9: Erdmann Heise, Bodo Ritter, Reinhold Schrodin (2006):
Operational Implementation of the Multilayer Soil Model

No. 10: M.D. Tsyrulnikov (2007):
Is the particle filtering approach appropriate for meso-scale data assimilation?

No. 11: Dmitrii V. Mironov (2008):
Parameterization of Lakes in Numerical Weather Prediction. Description of a Lake Model.

No. 12: Adriano Raspanti (2009):
Final report on priority project VERSUS (VERification System Unified Survey).

No. 13: Chiara Mirsigli (2009):
Final report on priority project SREPS (Short Range Ensemble Prediction System).

No. 14: Michael Baldauf (2009):
COSMO Priority Project "Further Developments of the Runge-Kutta Time Integration Scheme" (RK); Final Report.

No. 15: Silke Dierer (2009):
COSMO Priority Project "Further Developments of the Runge-Kutta Time Integration Scheme" (RK); Final Report.

No. 16: Pierre Eckert (2009):
COSMO Priority Project "INTERP"; Final Report.

No. 17: D. Leuenberger, M. Stoll, A. Roches (2010):
Description of some convective indices, implemented in the COSMO model.

No. 18: Daniel Leuenberger (2010):
Statistical Analysis of high-resolution COSMO Ensemble forecasts, in view of Data Assimilation.

No. 19: A. Montani, D. Cesari, C. Marsigli, T. Paccagnella (2010):
Seven years of activity in the field of mesoscale ensemble forecasting by the COSMO-LEPS system: main achievements and open challenges.

No. 20: A. Roches, O. Fuhrer (2012):
Tracer module in the COSMO model.

No. 21: M. Baldauf (2013):
A new fast-waves solver for the Runge-Kutta dynamical core.

No. 22: C. Marsigli, T. Diomede, A. Montani, T. Paccagnella, P. Louka, F. Gofa, A. Corigliano (2013):
The CONSENS Priority Project.

No. 23: M. Baldauf, O. Fuhrer, M. J. Kurowski, G. de Morsier, M. Muellner, Z. P. Piotrowski, B. Rosa, P. L. Vitagliano, D. Wojcik, M. Ziemianski (2013):
The COSMO Priority Project 'Conservative Dynamical Core' Final Report.

No. 24: A. K. Miltenberger, A. Roches, S. Pfahl, H. Wernli (2014):
Online Trajectory Module in COSMO: A short user guide.

No. 25: P. Khain, I. Carmona, A. Voudouri, E. Avgoustoglou, J.-M. Bettems, F. Grazzini (2015):
The Proof of the Parameters Calibration Method: CALMO Progress Report.

No. 26: D. Mironov, E. Machulskaya, B. Szintai, M. Raschendorfer, V. Perov, M. Chumakov, E. Avgoustoglou (2015):
The COSMO Priority Project 'UTCS' Final Report.

No. 27: Jean-Marie Bettems (2015):
The COSMO Priority Project 'COLOBOC' Final Report.

No. 28: Ulrich Blahak (2016):
RADAR_MIE_LM and RADAR_MIELIB - Calculation of Radar Reflectivity from Model Output.